Synthesis, Biological Evaluation, and Molecular Modeling of 1-Benzyl-1H-imidazoles as Selective Inhibitors of Aldosterone Synthase (CYP11B2)

Luc Roumen,[†] Joris W. Peeters,[‡] Judith M. A. Emmen,[§] Ilona P. E. Beugels,[§] Erica M. G. Custers,[‖] Marcel de Gooyer,[⊥] Ralf Plate,[‖] Koen Pieterse,[†] Peter A. J. Hilbers,[†] Jos F. M. Smits,[§] Jef A. J. Vekemans,[‡] Dirk Leysen,[§] Harry C. J. Ottenheijm,[§] Henk M. Janssen,[‡] and J. J. Rob Hermans*,[§]

[†]*BioModeling and bioInformatics, Eindhoven University of Technology, PO Box 513, Eindhoven 5600 MB, The Netherlands,* [‡]*SyMO-Chem BV, Den Dolech 2, Eindhoven 5612 AZ, The Netherlands,* [§]*Department of Pharmacology and Toxicology, Cardiovascular Research Institute Maastricht, Maastricht University, P.O. Box 616, Maastricht 6200 MB, The Netherlands,* [‖]*Department Medicinal Chemistry, Schering-Plough Research Institute, P.O. Box 20, Oss 5340 BH, The Netherlands, and* [⊥]*Department of Pharmacology, Schering-Plough Research Institute, P.O. Box 20, Oss 5340 BH, The Netherlands*

Reducing aldosterone action is beneficial in various major diseases such as heart failure. Currently, this is achieved with mineralocorticoid receptor antagonists, however, aldosterone synthase (CYP11B2) inhibitors may offer a promising alternative. In this study, we used three-dimensional modeling of CYP11B2 to model the binding modes of the natural substrate 18-hydroxycorticosterone and the recently published CYP11B2 inhibitor *R*-fadrozole as a rational guide to design 44 structurally simple and achiral 1-benzyl-1H-imidazoles. Their syntheses, in vitro inhibitor potencies, and in silico docking are described. Some promising CYP11B2 inhibitors were identified, with our novel lead MOERAS115 (4-((5-phenyl-1H-imidazol-1-yl)methyl)benzonitrile) displaying an IC_{50} for CYP11B2 of 1.7 nM, and a CYP11B2 (versus CYP11B1) selectivity of 16.5, comparable to *R*-fadrozole (IC_{50} for CYP11B2 6.0 nM, selectivity 19.8). Molecular docking of the inhibitors in the models enabled us to generate posthoc hypotheses on their binding modes, providing a valuable basis for future studies and further design of CYP11B2 inhibitors.

Introduction

The mineralocorticoid hormone aldosterone is an important regulator of the sodium and potassium balance, extracellular fluid volume, and blood pressure. It exerts its biological effects via (classical) genomic as well as nongenomic (rapid) actions that are mainly due to interaction with the mineralocorticoid receptor (MR[a]), although interaction with alternative but yet to be identified receptors may also contribute to the effects of aldosterone.[1]

Apart from its role in physiology, aldosterone seems to play a prominent role in the pathogenesis of various diseases as, e.g., heart failure,[2] arrhythmias,[2] hypertension,[3] nephropathy,[4,5] and edema.[6] In particular, in the case of chronic heart failure or postmyocardial infarction, clinical studies have convincingly shown benefit of blocking the action of aldosterone with MR antagonists and a reduction of patient mortality.[7,8]

As we and others[9] have put forward, an alternative manner to reduce aldosterone action is to inhibit its biosynthesis. This approach may solve the problems associated with MR antagonism such as side-effects,[10] interindividual variations in patient response regarding the pharmacodynamics and pharmacokinetics of MR antagonists,[11] and the induced compensatory aldosterone synthesis of which long-term effects are unknown.[10,12] The latter might be of relevance in view of the fact that not all aldosterone actions seem to involve the mineralocorticoid receptor.[2]

Aldosterone is mainly produced in the adrenal cortex, where its biosynthesis from the precursor cholesterol involves a number of catalytic steps and enzymes (Figure 1).[13,14] The early steps of aldosterone biosynthesis share pathways and precursors with other steroidal hormones. The final steps of aldosterone biosynthesis are conducted by the cytochrome P450 enzymes 11B1 (cortisol synthase) and 11B2 (aldosterone synthase), which will further be denoted as CYP11B1 and CYP11B2, respectively. These enzymes catalyze the 11-hydroxylation of 11-deoxycorticosterone to corticosterone, which is then further hydroxylated to 18-hydroxycorticosterone (18OH-B). Finally, CYP11B2 (but not CYP11B1) oxidizes the 18-hydroxyl group of 18OH-B to the corresponding aldehyde, thus resulting in the formation of aldosterone.

CYP11B1 shows a high structural overlap with CYP11B2 and shares some ligand conversion features with the latter (Figure 1). However, CYP11B1 is mainly responsible for glucocorticoid formation.[13,14] Thus, to obtain specific inhibition

*To whom correspondence should be addressed. Phone: +31 433 88 1331. Fax: +31 433 88 4149. E-mail: r.hermans@farmaco.unimaas.nl.

[a] Abbreviations: CYP11B1 and −11B2, cytochrome P450 11B1 and −2, respectively; MR, mineralocorticoid receptor; 18OH-B, 18-hydroxycorticosterone; B1model_Sfad, CYP11B1 model optimized with *S*-fadrozole; B1model_18OHB, CYP11B1 model optimized with 18-hydroxycorticosterone; B2model_Rfad, CYP11B2 model optimized with *R*-fadrozole; B2model_18OHB, CYP11B2 model optimized with 18-hydroxycorticosterone; MD, molecular dynamics; LC-MS, liquid chromatography−mass spectrometry; GC-MS, gas chromatography−mass spectrometry; HPLC, high performance liquid chromatography; LOO, leave-one-out.
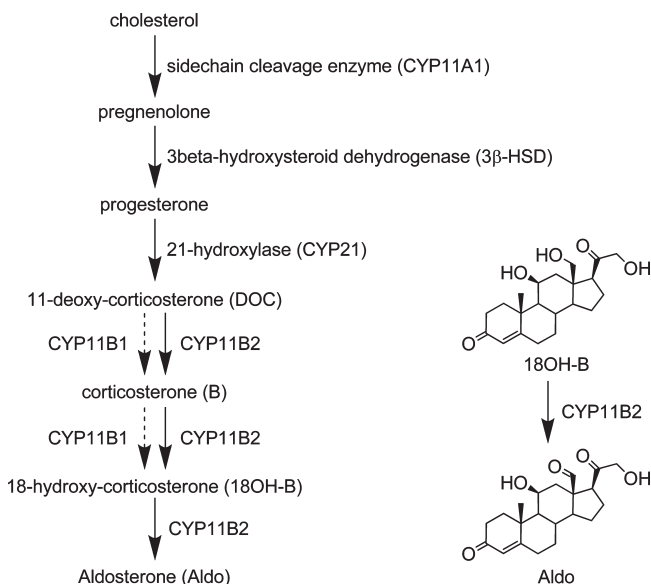
Figure 1. Final steps of the biosynthesis of aldosterone by the CYP11B family.

of the biosynthesis of aldosterone, it is essential to focus on CYP11B2 and to avoid extensive CYP11B1 inhibition.

Recently, *R*-fadrozole (also referred to as FAD286) was identified as a CYP11B2 inhibitor[15] (Table 1). Animal studies have shown that *R*-fadrozole does indeed lower aldosterone levels in vivo and that it reduces end organ damage and pathologies in which aldosterone is known to play a role, i.e., cardiac fibrosis,[16,17] kidney fibrosis,[4] primary aldosteronism,[18] cardiac hypertrophy,[15] diabetes associated cardiac arrythmias and nephropathy,[19,20] and salt-induced hypertension and sympathetic hyperactivity.[21] This indicates that CYP11B2 is indeed a promising drug target.

Apart from *R*-fadrozole or its analogues, a number of specific CYP11B2 inhibitors have been described. For instance, Hartmann et al. described a variety of compounds featuring an aromatic heterocycle such as a pyridine,[22−24] an imidazole,[23,24] or an isoquinoline moiety,[25] which are thought to strongly interact with the cytochrome heme iron atom (Supporting Information Figure 1). These hypothesized interactions between the ligand and the heme iron are based on interactions of nitrogen containing aromatic heterocycles as shown in numerous crystal structures of cytochrome P450 enzymes combined with their ligands (see review de Graaf et al.[26]). Furthermore, the aromatic moieties designed by Hartmann et al. are linked either directly or via a methylene group to two fused rings that are provided with various substituents. Recently, structures featuring a pyridine moiety have been optimized through 3,6- and 3,7-substitution (Supporting Information Figure 1, compound **D**)[27] and those featuring an isoquinoline moiety through introduction of a dihydroquinolinone.[28]

In the present study, we aim at the design and synthesis of a different class of CYP11B2 inhibitors: structurally relatively simple nonchiral 1-benzyl-1*H*-imidazoles that, in contrast to the fadrozoles or the above-mentioned compounds of the group of Hartmann, do not contain fused ring systems and chiral carbon atoms. Using an in silico modeling approach, we have designed a number of compounds that were subsequently synthesized and tested for their ability to inhibit human CYP11B2 and CYP11B1 in an in vitro assay. As a rational basis for CYP11B2 inhibitor design, we have used our

Table 1. In Vitro Binding Potencies in CYP11B1 and CYP11B2 for the Synthesized Inhibitors

Compound	X	Y	CYP11B1 binding IC50 (nM)	CYP11B2 binding IC50 (nM)	CYP11B2 *versus* CYP11B1 Selectivity (-)
1a	H	H	709 ± 68	1799 ± 332	0.4
1b	4-CN	H	368 ± 93	372 ± 245	1.0
1c	4-F	H	494 ± 31	330 ± 231	1.5
1d	4-Cl	H	>1000	>1000	-
1e	4-Br	H	211 ± 14	479 ± 24	0.4
1f	4-CH$_2$OH	H	695 ± 73	>1000	-
1g	4-NH$_2$	H	236 ± 50	>1000	-
2b	3-CN	H	>1000	>1000	-
2c	3-F	H	206 ± 40	815 ± 23	0.3
2d	3-Cl	H	151 ± 20	457 ± 29	0.3
2e	3-Br	H	143 ± 99	365 ± 100	0.4
2f	3-CH$_2$OH	H	206 ± 1.5	1174 ± 221	0.2
2g	3-NH$_2$	H	390 ± 90	600 ± 125	0.7
3a	H	C$_2$H$_4$COOCH$_3$	326 ± 18	193 ± 18	1.7
3b	4-CN	C$_2$H$_4$COOCH$_3$	31 ± 6.1	3.5 ± 0.6	8.9
3c	4-F	C$_2$H$_4$COOCH$_3$	104 ± 7.8	50 ± 7.8	2.1
3d	4-Cl	C$_2$H$_4$COOCH$_3$	123 ± 30	177 ± 53	0.7
3e	4-Br	C$_2$H$_4$COOCH$_3$	57 ± 5.6	4.0 ± 0.5	14.3
3h	4-OCH$_3$	C$_2$H$_4$COOCH$_3$	111 ± 31	121 ± 45	0.9
4a	H	C$_3$H$_6$OH	181 ± 18	286 ± 26	0.6
4b	4-CN	C$_3$H$_6$OH	48 ± 20	13 ± 4.9	3.7
4c	4-F	C$_3$H$_6$OH	116 ± 6.3	16 ± 3.2	7.3
4d	4-Cl	C$_3$H$_6$OH	44 ± 0.4	55 ± 1.2	0.8
4e	4-Br	C$_3$H$_6$OH	18 ± 4.0	6.2 ± 0.9	2.9
4h	4-OCH$_3$	C$_3$H$_6$OH	12 ± 2.0	59 ± 2.8	0.2
5a	H	Ph	4.8 ± 0.6	11 ± 2.7	0.4
5b	4-CN	Ph	28 ± 3.5	1.7 ± 0.6	16.5
5c	4-F	Ph	16 ± 5.3	11 ± 1.5	1.5
5d	4-Cl	Ph	25 ± 15	5.8 ± 1.6	4.3
5e	4-Br	Ph	7 ± 1.8	5.1 ± 2.0	1.4
5h	4-OCH$_3$	Ph	11 ± 0.9	14 ± 2.1	0.8
6a	4-CN	CH$_2$OCOCH$_3$	213 ± 17	44 ± 10	4.8
6b	4-CN	COOCH$_3$	48 ± 21	7 ± 6.7	6.8
6c	4-CN	CH$_3$	141 ± 42	12 ± 4.3	11.8
6d	4-CN	Br	73 ± 6.9	23 ± 6.5	3.2
6e	4-CN	HCO	478 ± 373	62 ± 5.4	7.7
6f	4-CN	CH$_2$OH	285 ± 29	29 ± 3.7	9.8
6g	4-CN	[pyridinylmethyl]	307 ± 23	407 ± 38	0.8
7a	4-CN	[2-F-benzyl]	20 ± 3.4	2.3 ± 0.5	8.7
7b	4-CN	[benzyl]	5.7 ± 2.2	3.7 ± 3.4	1.5
7c	4-CN	[3-F-benzyl]	32 ± 8.5	5.5 ± 1.0	5.8
7d	4-CN	[3-methylbenzyl]	6.2 ± 2.4	5.2 ± 5.2	1.2
7e	4-CN	[4-F-benzyl]	27 ± 8.6	25 ± 5.1	1.1
7f	4-CN	[4-methylbenzyl]	130 ± 79	117 ± 14.6	1.1
R-fadrozole			119 ± 8.9	6.0 ± 1.9	19.8
S-fadrozole			40 ± 4.4	171 ± 5.1	0.2
R-etomidate			0.5 ± 0.2	1.7 ± 0.9	0.3

published three-dimensional CYP11B1 and CYP11B2 models.[29] These models have previously been compared to those of Ulmschneider et al.[30] and of Belkina et al.[31] and have proven to accurately describe protein−substrate interactions and protein−inhibitor interactions such as with *R*- and *S*-fadrozole and *R*-etomidate, another well-known CYP11B inhibitor.[32] In designing the 1-benzyl-1*H*-imidazoles as CYP11B2 inhibitors, we have combined the modeled *R*-fadrozole interaction with the structural investigation of the protein−inhibitor interactions by performing molecular docking in the CYP11B1 and CYP11B2 models. The ligand poses resulting from the molecular docking analyses have subsequently been used in a retrospective analysis to rationalize the structure−activity
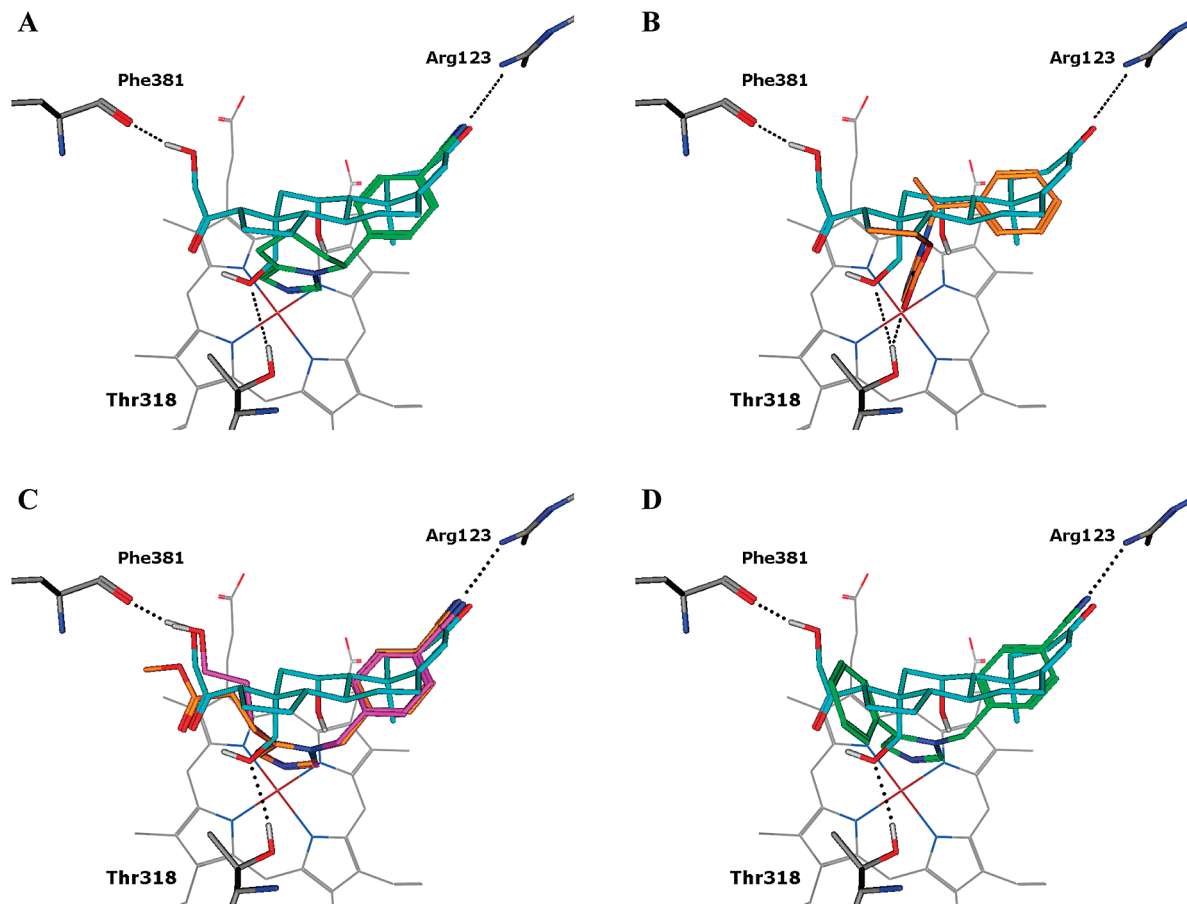
Figure 2. Three-dimensional overlays of 18-hydroxycorticosterone (cyan) in the active site of CYP11B2 with (A) *R*-fadrozole (green), (B) *R*-etomidate (orange), (C) the 5-methyl propanoate substituted 4-cyanobenzyl-1*H*-imidazole (**3b**, orange) and the 5-propanol substituted 4-cyanobenzyl-1*H*-imidazole (**4b**, purple), and (D) the 5-phenyl substituted 4-cyanobenzyl-1*H*-imidazole (**5b**, green). 2D structural formulas of the inhibitors can be found in Table 1.

relationship of the synthesized compounds. Because the protein models feature a rigid structure, various protein conformations[29] were included in our docking analysis to account for possible active site perturbations. If the docking protocol showed a sufficient trend with the pIC_{50}, these protein structures were further analyzed to determine which active site features they contained that might be of importance for protein−ligand interactions.

Results

Rationale for the Inhibitor Design. As a starting point for the inhibitor design, we have compared the interaction of the natural ligand 18-hydroxycorticosterone (18OH-B) in the active site of the CYP11B2 model with the modeled interactions of the two CYP11B2 inhibitors *R*-fadrozole (Figure 2A, green) and *R*-etomidate (Figure 2B, orange).[29] In these models, the binding mode of 18OH-B is stabilized by the formation of the following three hydrogen bond interactions with the protein active site: (1) between the C_3 carbonyl and Arg123, (2) between the C_{21}-hydroxyl group and the Phe381 backbone, and (3) between the C_{18}-hydroxyl group and Thr318. In addition, the natural ligand possesses an internal hydrogen bond between its C_{18}-hydroxyl and its C_{20}-carbonyl groups. Modeling of *R*-fadrozole shows that this inhibitor strongly binds to the heme iron atom with its aromatic nitrogen atom and that it mimics the interaction of 18OH-B with Arg123 via its nitrile group. When modeling *R*-etomidate, we observed that this ligand also strongly binds to the heme

iron but in contrast to *R*-fadrozole possesses the interaction with Thr318.

Next, we designed three main modifications for the *R*-fadrozole structure to mimic the interactions of the steroid. These substituents are placed at the 5-position of the benzyl-imidazole group and are the introduction of a methyl *n*-propanoate moiety (Figure 2C purple, Table 1 series **3**), an *n*-propanol moiety (Figure 2C orange, Table 1 series **4**), and a phenyl group (Figure 2D green, Table 1 series **5**), respectively. The *n*-propanol moiety is overlaid with the C_{21}-hydroxyl group of 18OH-B, the methyl *n*-propanoate moiety with the C_{20}-carbonyl group of 18OH-B, and the phenyl group partially fills the space of the D-ring of 18OH-B as well as the $C_{20,21}$-hydroxyacetyl group of 18OH-B. The resulting 5-imidazole substituted analogues were further modified by replacing the nitrile group present in *R*-fadrozole. We also opted for designing compounds that do or do not mimic the interaction with Thr318 that is characteristic for *R*-etomidate. Thereby, the importance of this type of interaction with Thr318 can be elucidated. All of the compounds that were synthesized for this investigation possess the 4-nitrile benzyl group that is present in *R*-fadrozole. An overview of all the compounds that have been synthesized and tested for CYP11B2 and -11B1 inhibition are listed in Table 1.

Synthesis. The *N*-benzyl imidazole compounds **1b−e** and **2b−e** have been prepared by alkylation of imidazole with the appropriate substituted benzyl bromides, providing the products in isolated yields of 32−68%. Compounds **1g** has been

Scheme 1. Synthesis of the Imidazole Series **3** and **4** from Urocanic Acid **11**[33][a]
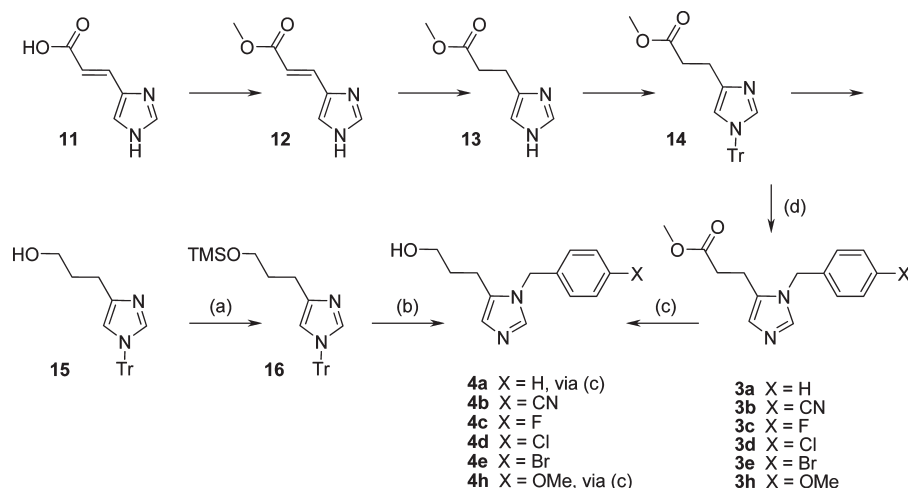
[a] (a) TMS-Cl, Et$_3$N, CHCl$_3$, RT, 1 h; (b) (i) corresponding 4-substituted benzyl bromides **10**, acetonitrile, 55−80 °C, 18 h, (ii) acetic acid, water, reflux, 10 min; (c) LiAlH$_4$, THF, 0 °C; (d) (i) corresponding 4-substituted benzyl bromide, acetonitrile, 55−80 °C, 18 h, (ii) MeOH, reflux, 30 min.

Scheme 2. Synthesis of the Imidazole Series **5** and **6** from Substituted Imidazoles[a]
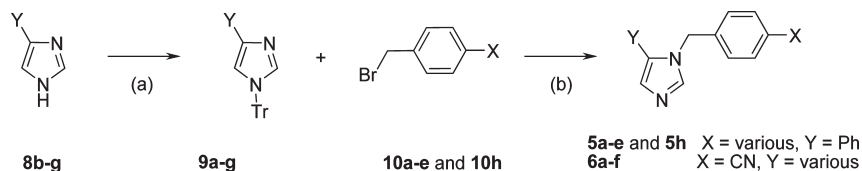
[a] (a) ClCPh$_3$, Et$_3$N, CHCl$_3$, RT, 1 h; (b) (i) acetonitrile, CHCl$_3$, 80 °C, 18 h, (ii) acetic acid, H$_2$O, reflux, 10 min.

Scheme 3. Synthesis of Imidazole **6g** and the Series **7** by Suzuki Coupling Reactions[a]
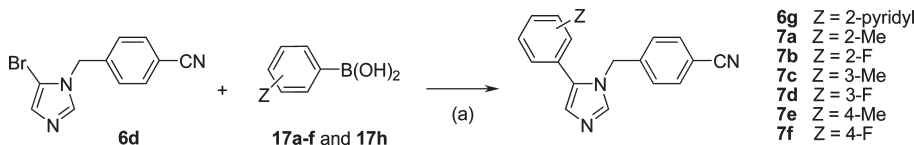
[a] (a) DME, EtOH, water, Na$_2$CO$_3$, Pd(PPh$_3$)$_4$, 75 °C, 18 h.

derived from its nitro precursor by a catalytic hydrogenation reaction. The syntheses of the other inhibitors prepared are outlined in Schemes 1−Scheme 3. The tritylated imidazole building blocks **14** and **16** have been made in high-yielding steps from urocanic acid **11** by using procedures as described by Stark et al. (see Scheme 1).[33] The methyl ester **14** has been N-alkylated with a series of benzyl bromides, followed by removal of the trityl group, to acquire compounds **3a−e** and **3h**. Similarly, the imidazole derivative **16** has been benzylated and detritylated to prepare inhibitors **4b−4e**. In an alternative synthetic approach, the methyl esters **3a** and **3h** have been reduced to give the alcohols **4a** and **4h** in good yields.

Commercially available phenyl imidazole can conveniently be tritylated to provide building block **9g**, enabling subsequent N-alkylation with various benzyl bromides to furnish the series of compounds **5**, while other commercially available substituted imidazoles have also been tritylated and then converted with 4-cyano benzyl bromide to prepare compounds **6a−6e** (see Scheme 2). The isolated yields for the applied alkylations−deprotections of the tritylated imidazoles to acquire the series of compounds **3**, **4**, **5**, and **6** depend on the specific reactants and can vary between 11% and 100%, but are typically around 50%. Compound **6f** has been

made from **6a** by hydrolysis of the ester group. Finally, compound **6g** and the series of compounds **7a−f** have been prepared in isolated yields between 35% and 89% by a Suzuki coupling reaction of the bromide **6d** and the appropriate aryl boronic acids (Scheme 3).

Even though these prepared 1-benzyl-1*H*-imidazoles are simple in structure and bear resemblance to the well-known fadrozole structure, quite a number of the presented molecules are novel, in particular those with aryl groups in the R5-position of the imidazole ring, such as most molecules in the **5** and **7** series, and molecule **6g**.

In Vitro Screening. The compounds were tested as inhibitors of human CYP11B1 and CYP11B2 in an in vitro screening method. This method consisted of an incubation of test compounds and the substrate 11-deoxycorticosterone with cultured V79 cells that stably overexpress CYP11B1 or CYP11B2,[34−36] followed by HPLC analysis of cell medium extracts to determine substrate conversion rates. The obtained IC$_{50}$ values are shown in Table 1.

Overall, the IC$_{50}$ values of the inhibitors range from as low as 0.5 nM to more than 1000 nM (i.e., the highest tested inhibitor concentrations). The CYP11B2 versus CYP11B1 selectivity defined as the quotient of the IC$_{50}$ values for CYP11B1 and CYP11B2 varies from 0.2 to 16.5. The most

potent CYP11B2 inhibitors are **3b**, **3e**, **4e**, **5b**, **5d**, **5e**, **6b**, and **7a**–**d** (IC$_{50}$ < 10 nM), whereas the most selective CYP11B2 inhibitors are **3b**, **3e**, **4c**, **5b**, **5d**, **6a**, **6b**, **6c**, **6e**, **6f**, **7a**, and **7c** (selectivity > 4). The most potent CYP11B1 inhibitors are 5a, **5e**, **7b**, and **7d**, whereas the most selective CYP11B1 inhibitors are **2c**, **2f**, and **4h**.

Inspection of the IC$_{50}$ values of the para- and meta-substituted series **1a**–**g** and **2b**–**g** shows that these series are not very potent for CYP11B2 and generally better inhibitors for CYP11B1. Meta substitution seems to yield an inhibitor that is selective for CYP11B1. For the para substituted compounds (**1a**–**g**), this does not seem to be a general rule because marginal selectivity for CYP11B2 is observed when the para-substituent is a fluoride group (selectivity of 1.5), while no selectivity is seen (selectivity = 1) when it is a nitrile group. Importantly, if a substituent is introduced at the 5-position of the imidazole group, the CYP11B2 potency generally is markedly increased as is the selectivity.

Investigation of series **3a**–**e**, **3h**, **4a**–**e**, **4h**, and **5a**–**e**, **5h**, reveals that within these series, the nitrile, fluoride, and bromide groups are profitable for both CYP11B2 potency (2–50 nM) as well as CYP11B2 versus CYP11B1 selectivity (factor 1.4–16.5). For compounds **3e** and **5b**, the CYP11B2 versus CYP11B1 selectivity even approaches that of *R*-fadrozole (factor 19.8). It is striking that of the compounds **3c**–**e** and **4c**–**e**, the chloride bearing analogues **3d** and **4d** have the lowest CYP11B2 potency. Comparing the CYP11B2 potencies, it is clear that both the bromide and nitrile substituents are most favored in the active site of CYP11B2. Overall, the bromide substituent also infers the best CYP11B1 potency.

The introduction of other 5-imidazole substituents (series **6a**–**g**) also increases the potency and selectivity for CYP11B2. Comparing the potency of *R*-etomidate to **6b** shows a slightly decreased potency for CYP11B1 as well as for CYP11B2. The drop in potency is larger for CYP11B1, which can be attributed to the introduction of the nitrile group that seems to be suboptimal for binding to CYP11B1. Introduction of a sterically small substituent (e.g., **6c**) leads to increased selectivity for CYP11B2; however, when a hydrogen bond donor (**6f**) or acceptor (**6e**) is added, neither an increase of potency nor an increase of selectivity is observed. The introduction of a methyl substituent confers more selectivity than the introduction of a propanoate (**3b**) and propanol (**4b**) but less selectivity than the phenyl group (**5b**) (compare the selectivity of 11.8 to 8.9, 3.7, and 16.5, respectively).

Molecular Docking. Validation of the Docking Procedure. In addition to the design, synthesis, and biological testing of the inhibitors presented in this study, we have investigated the binding mode of the inhibitors in the three-dimensional models of CYP11B1 and CYP11B2, respectively. For the evaluation of the binding mode of the inhibitors, flexible docking has been carried out on several different protein conformations extracted from molecular dynamics simulations presented in an earlier study.[29] The molecular dynamics of the CYP11B1 and CYP11B2 models have been performed with either 18-hydroxycorticosterone (models will be denoted as B1model_18OHB and B2model_18OHB, respectively) or fadrozole. The CYP11B1 model contains the *S*-enantiomer in the active site (denoted as B1model_Sfad), whereas the CYP11B2 model contains the *R*-enantiomer in the active site (denoted as B2model_Rfad). We have

specifically chosen *S*-fadrozole in combination with CYP11B1 because it is a strong and selective inhibitor for this isoform (Table 1).[29]

The docking results of the ligands in all of the four initial optimized structures (homology models) can be seen in Figure 3. In our previous modeling study, we have observed a trend between the GoldScore and the IC$_{50}$. Because the GoldScore is an artificial fitness function, we have investigated the occurrence of chance correlation between the docking score and the potency (Supporting Information Figures 2 and 3). To validate the docking procedure in the CYP11B homology models, regression analysis has been carried out for the GoldScore and the binding affinity of the compounds (Table 2). This analysis suggests that a relation between the GoldScore of our docked compounds and the pIC$_{50}$ exists. Hence, we have decided that the trend between the GoldScore and pIC$_{50}$ can be used to select protein conformations from the MD study, which may possess active site features that related to the SAR of the synthesized compounds.

The regression analysis showed that compound **6g** is a clear outlier in the docking. On the basis of the consideration that the GoldScore does not discriminate any electrostatic properties of the pyridine and phenyl moieties, compound **6g** is consistently scored equal to the more potent phenyl analogue **5b**. Because the GoldScore cannot capture the behavior of the ring and the electrostatic interactions of the ring are likely to play a role in protein–ligand interactions, we have decided to leave compound **6g** out of the analysis. Indeed, by doing so, the obtained correlation was significantly improved (*P* < 0.05 for all models in F-test), such that we find the omission of compound **6g** justified. The characteristics of the regression analysis seem sufficient to conclude that our CYP11B models may be used to rationalize structure–activity relationships in a posthoc fashion (Table 2, R^2 > 0.75, q^2_{LOO} > 0.75, and $q^2_{k\text{-fold}}$ > 0.7).

Molecular Dynamics and the Effect of the Choice of Ligand Used for Model Optimization on Docking Performance. Investigation of the various protein conformations of the CYP11B1 and CYP11B2 models reveals that around half of the protein conformations sampled by the molecular dynamics (MD) simulations possess a similar trend between the GoldScore and the pIC$_{50}$ as the original models. Hence, they seem feasible for the docking, ranking, and scoring of the inhibitors synthesized and for generating hypotheses on active site features that may determine protein–ligand interactions (Supporting Information Figure 4). During the MD, the protein conformation remained steady, resulting in several protein conformations in which the docking poses are seemingly in line with the observed IC$_{50}$s. Only the B1model_Sfad had in the MD several successive protein conformations in which the relationship between the Gold-Score and the pIC$_{50}$ is lost (conformations 15–22). However, generally speaking, all of the homology models possess an adequate performance for docking.

If for CYP11B1 18OH-B was used as a ligand in our homology models (B1model_18OHB), the performance of the homology models in their basal conformation (conformation 1) was poorer than if *S*-fadrozole was used (B1model_Sfad). Also, if the various MD conformations were compared for the basal B1model_18OHB, MD conformation 23 seemed to perform better in the inhibitor dockings than the basal B1model_18OHB. A possible reason for this is that while 18OH-B is not a substrate for CYP11B1,
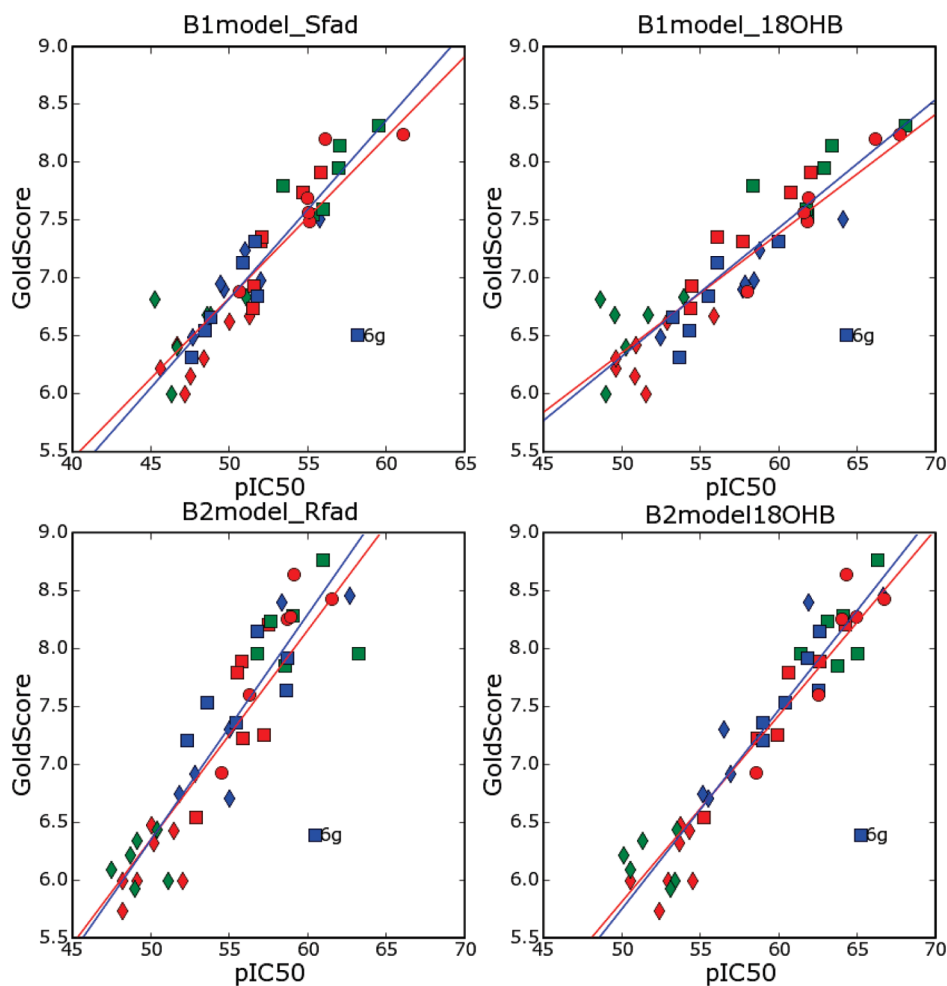
Figure 3. Relation between the GoldScore and the pIC$_{50}$ of the inhibitors in the four optimized protein structures of (A) B1model_Sfad, (B) B1model_18OHB, (C) B2model_Rfad, and (D) B2model_18OHB. Red diamonds, series **1**; green diamonds, series **2**; blue diamonds, series **3**; red squares, series **4**; green squares, series **5**; blue squares, series **6**; red circles, series **7**. The red line indicates the line corresponding to the original regression model (see Table 1, Supporting Information), whereas the blue line corresponds to the regression model without outlier **6g**.

Table 2. Correlation Data for the Formulae of the GoldScore in Relation to the pIC$_{50}$ Values for the Different Models as pIC$_{50}$ = A × GoldScore + B[a]

| model	A	B	R^2	q^2 LOO	S_{PRESS} LOO	q^2 k-fold	S_{PRESS} k-fold	F
B1model_Sfad	0.154 ± 0.002	-0.877 ± 0.096	0.865	0.848	0.250	0.846	0.252	261.639
B1model_18OHB	0.111 ± 0.002	0.772 ± 0.126	0.849	0.833	0.262	0.832	0.263	230.477
B2model_Rfad	0.195 ± 0.001	-3.404 ± 0.070	0.846	0.828	0.377	0.826	0.379	225.126
B2model_18OHB	0.172 ± 0.001	-2.853 ± 0.083	0.919	0.910	0.273	0.716	0.443	462.659

[a] k-Fold is taken as 1000 times a k-fold cross-validation with k = 20% of the data set. Outlier **6g** is not included in these formulas. Regression constants are the correlation coefficient (R^2), the cross-validated correlation coefficient (q^2), the standard error (S), test statistic (F), and the prediction error sum of squares (PRESS).

it fills a larger portion of the active site pocket than *S*-fadrozole, especially around Phe381 (compare Figure 2A and Figure 4). The MD conformation of 18OH-B pushes Phe558 to the top of the active site, whereas in the MD conformation of *S*-fadrozole, Phe558 forms a neat packing to narrow the pocket. The docking of ligands in the narrow pocket is more favorable than in the larger cavity in which the ligands can fit more flexibly. In addition, a narrow pocket probably will also result in a better ranking because the GoldScore is optimized for steric interactions. To summarize, molecular dynamics of the B1model_18OHB has evolved the active site to conformation 23, of which the active site conformation is comparable to that of the B1model_Sfad (rmsd of Phe558 side chain is 0.5 Å, data not shown).

For CYP11B2, B2model_18OHB performs better in the docking of the inhibitors synthesized than the B2model_R-fad. Both models show a similar active site packing (Figure 5). The active site influences causing this difference in ranking effectiveness are more subtle than for the protein conformations of CYP11B1 and cannot be easily rationalized.

Observed Inhibitor−Protein Interactions in the Docking Studies. Docked inside the B2model_18OHB, the compounds **4a−e** and **4h** interact with the protein backbone carbonyl of Phe381 via its *n*-propanolyl moiety. In addition, the docking pose of compound **4b** possesses a stabilizing interaction with Arg123 (Figure 5). These interactions are similar to the ligand-based design discussed in the Rationale section. The compounds **3a−e** and **3h** all fit with the propano-ate group in its extended conformation as is demonstrated
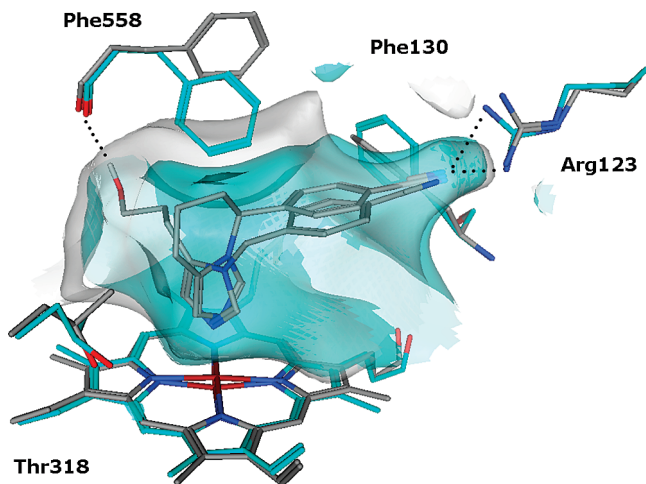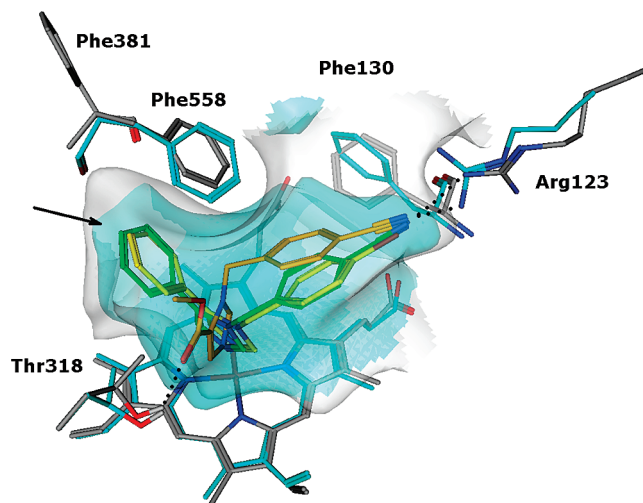
Figure 4. Active site difference between the CYP11B1 model optimized with *S*-fadrozole (cyan) and 18OH-B (white). The molecules shown in the active site are *S*-fadrozole and **4b**. The induced fit of *S*-fadrozole features a movement of Phe558, narrowing the active site pocket.
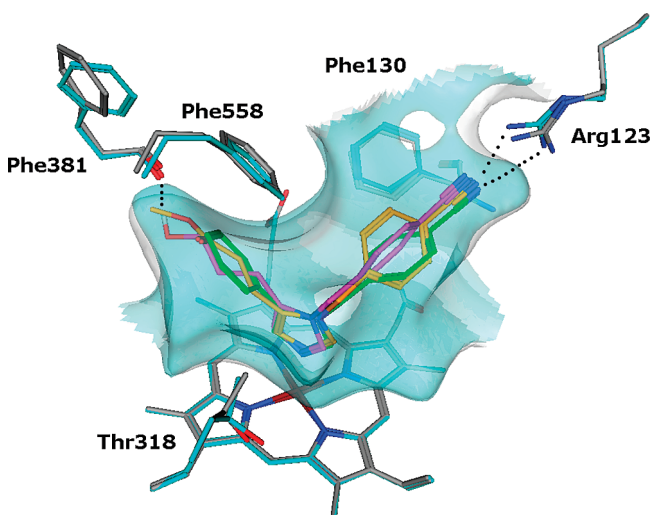
Figure 5. Active site differences for CYP11B2 optimized with *R*-fadrozole (cyan) and 18OH-B (white). Only very small active site differences are observed. Inside the cavity, the docking results for compounds **3b** (orange), **4b** (purple), and **5b** (green).

for compound **3b** in Figure 5. As such, these compounds are not docked in the active site pocket as anticipated in the design of mimics for the C_{20}-carbonyl group of 18OH-B. In retrospect, this is understandable because the C_{20}-carbonyl group of the steroid is stabilized by the internal hydrogen bond with its C_{18}-hydroxyl group, but this particular interaction is absent in case of the inhibitors.

Instead of the designed curled conformation, the *n*-propanoate moiety adopts a flat orientation in the active site pocket similar to the phenyl ring of compounds **5a**−**e** and **5h**. This orientation is visualized in Figure 5 for compound **5b**. The compounds from series **5** and **7** all form stable ring stacking interactions with their phenyl moiety and Phe558, forming an out-of-plane rotation with respect to the imidazole ring. With regard to the phenyl ring of Phe558, there is room for the introduction of ortho and meta substituents, whereas the para position allows only limited substitution for the CYP11B2 models. This is indicated with an arrow for compound **5b** in Figure 6.

Figure 6. Active site differences between CYP11B1 optimized with *S*-fadrozole (cyan) and CYP11B2 optimized with 18OH-B (white). Indicated are the docking poses of **5b** (green), **5e** (yellow), and **6b** (orange) in the CYP11B2 model. The arrow indicates the limited volume around the para-position.

Because of the interaction with Phe558, the protrusion of the *para*-benzyl substituents toward Arg123 is limited. Figure 6 illustrates that the bromide substituent fits more comfortably into the CYP11B1 pocket than the nitrile, whereas the corresponding space of the pocket in CYP11B2 is larger (compare **5e** and **7f**). The binding orientation of the imidazole above the heme for series **6** is varying in accordance with the substituent size. The larger compounds **6a** and **6g** bind in a similar fashion as observed for the series **3**, **4**, **5**, and **7**. The other inhibitors bind with their small substituent oriented into the small pocket around Thr318, forming a hydrogen bond with the threonine alcohol if possible (see compound **6b**, Figure 6). The space around this substituent is similar for CYP11B1 and CYP11B2, although the pocket is slightly wider in CYP11B2. On the basis of these docking observations, we hypothesize that the compounds of series **6** are selective for CYP11B2 (versus CYP11B1) because of its more favorable pocket size for the *para*-nitrile substituent of these compounds near Arg123. No conclusions could be drawn from the docking results to explain the higher potency of compound **6c** over compounds **6e** and **6f**.

Discussion and Conclusion

The in silico design of novel CYP11B2 inhibitors based on its overlap with the steroid 18-hydroxycorticosterone has led to the synthesis of 1-benzyl-1*H*-imidazoles. The structures of these inhibitors are relatively simple, they are nonchiral, and they seem to achieve a good fit within the volume of the active site of CYP11B2. Of these 44 substances, 20 compounds possess a potency in the low nanomolar range (IC_{50} 1−30 nM) for CYP11B2 and 12 compounds for CYP11B1. In addition, nine compounds possess a considerable selectivity (versus CYP11B1) for CYP11B2 (5−20) that is close to that observed for *R*-fadrozole, a compound which has proven to be effective in vivo in reducing aldosterone levels and in reducing aldosterone related pathological events.[4,15−21] On the other hand, the CYP11B2 versus CYP11B1 selectivities of our compounds are quite poor when compared to those described by the group of Hartmann et al.[22−25] Their compounds possess scaffolds different from ours and display a selectivity

up to a 1000-fold. This shows that higher CYP11B2 versus CYP11B1 selectivity can be obtained but whether further optimization of the type of compounds that is described in the present study would indeed produce more selective compounds still awaits further investigation. Additionally, it has to be mentioned that in the present study, we have only screened for CYP11B1 and CYP11B2 inhibition. Given the quite simple structures of the compounds and their structural relationship with *S*-fadrozole (a known CYP19 inhibitor), it may well be that (some of) these compounds display inhibitory activity to the steroid converting enzymes CYP17 and CYP19. Future studies on optimizing the here described type of compounds for CYP11B2 inhibition should take this into account.

A molecular docking study of the inhibitors synthesized in various protein conformations has shown that our homology models are suitable to rationalize structure—activity relationships. In particular, the homology model of CYP11B1 optimized with *S*-fadrozole and that of CYP11B2 optimized with 18OH-B are the most appropriate for the structural investigation of fadrozole derivatives. Active site differences between these models near the amino acids Phe558, Thr318, and Arg123 have been shown to be important for ligand binding and ligand specificity. In particular, we propose that the use of a *para*-nitrile substituent on the benzyl ring leads to the highest CYP11B2 selectivity due to an interaction with Arg123 that is slightly different with the corresponding interaction in CYP11B1.

We have observed that a simultaneous substitution on the 5-imidazole and the 1-*H*-benzyl moieties does not lead to clear structure—activity relationships. Our models and docking investigations indicate that this may be due to the flexibility of the substituents placed on the 5-imidazole as in compound series **3** and **4**. The phenyl group of **5d** seems to fit more rigidly into the active site pocket of CYP11B2, thereby limiting the protrusion of the benzylimidazole moiety, locking the compounds of series **5** in one particular conformation. This locking is not observed with the compound series **3** and **4** where the imidazole is able to rotate freely.

In addition, we presume that the dual effect of polarizability as well as a spatial arrangement may play a role in the potency of the *para*-benzyl halogen containing inhibitors. The polar effects of the nitrile and fluoride groups allow these substituents to interact strongly with the Arg123 in the active site of our CYP11B2 models. On the other hand, based on our models, it seems that the large bromide substituent can form a weakly polar interaction with Arg123, and the *para*-bromide compounds possess a better steric fit in the active site pocket of CYP11B2. These various effects may play a role in the preferred docking of bromide compounds over fluoride and chloride compounds.

Overall, the bromide substituent also infers the corresponding ligands the higher CYP11B1 potency, often even higher than the corresponding nitrile bearing ligands (**1b,d**, **4b,e**, and **5b,d**, though not **3b,d**). Intuitively, the presence of a *para*-nitrile substituent ought to make a better interaction with Arg123, but for the tested compounds, this substituent protrudes further into the active site than a *para*-bromide substituent. This may indicate that in CYP11B1 the three-dimensional space close to Arg123 is more limited than in case of CYP11B2, as is in line with our earlier observations.[29] As such, the presence of a *para*-nitrile substituent seems to be a determining factor for the CYP11B2 selectivity of the benzyl-imidazoles.

Not all of the measured selectivities of the 5-substituted 1-benzyl-1*H*-imidazoles can be rationalized with the in silico models. For instance, the docking results are not able to rationalize the higher potency of compound **6c** over compounds **6e** and **6f**. Steric differences near Thr318 seem to have an effect, however, that does not explain why the ester group of compounds **6b** and *R*-etomidate does not result in a lower potency. Future optimizations of the homology models are required to shed light on these observations.

Finally, we propose that compound **5b**, compound code MOERAS115, is a good lead structure for future optimizations because in our models, it limits spatial movements of the flexible benzyl-imidazoles in the pocket of CYP11B2. It also possesses the important nitrile substituent on the para position of the benzyl moiety. Indeed, of the here-studied compounds, it possesses the highest CYP11B2 versus CYP11B1 selectivity (16.5) and a low IC_{50} value (1.7 nM) for CYP11B2. Early explorations of modifications of its 5-imidazole phenyl group and the molecular docking of these inhibitors (series **7**) have already given insight to the possibilities for structural optimization.

Experimental Section

Chemistry. Molecular characterization of the prepared compounds was performed by NMR spectroscopy using a Varian Mercury Vx 400 MHz or a Varian Gemini 300 MHz spectrometer, where spectra were recorded at a temperature of 298 K. Found coupling constants (*J*) are given in Hz. The purity of all products was determined using either LC-MS of GC-MS, where the chromatograms showed only a single peak corresponding to the desired product (purity ≥95%). LC-MS measurements were executed using a Finnigan LCQ Decca XP Max ESI-MS spectrometer and applying an Alltima HP C18 50 mm, 3 μm column with an acetonitrile/water eluent gradient, and 0.1% formic acid in the eluent for ionization. In addition to the MS-detection, photo diode array (PDA) detection was also performed. Some products have alternatively been characterized by GC-MS, using a Shimadzu GCMS-QP5000 spectrometer applying a Zebron ZB-5 15 m, 0.1 μm, or a Zebron ZB-35 30 m, 0.25 μm capillary column in a Shimadzu GC-17A chromatograph.

Compounds **1a**, **1f**, **2f**, **2g**, the substituted imidazoles **8**, the benzyl bromides **10**, urocanic acid **11**, and the aryl boronic acids **17** have been acquired from commercial sources (mainly Acros and Sigma-Aldrich). All further reagents, catalysts, chemicals, materials and solvents were also obtained commercially and were used without further purification. When appropriate, drying of solvents was done by applying molsieves that were prepared by drying in an oven at 500 °C.

The series of imidazoles **1** and **2** have been prepared using a similar procedure as that for compound **1c**. Details and changes with respect to the procedure for **1c** are given below.

1-(4-Fluorobenzyl)-1*H*-imidazole (1c). 4-Fluorobenzyl bromide **10c** (1.0 g, 5.3 mmol), imidazole (0.36 g, 5.3 mmol), and potassium carbonate (1.46 g, 10.6 mmol) were dissolved in 10 mL of acetonitrile and stirred for 4 h at 60 °C. After cooling down, the mixture was filtered and the filtrate was evaporated in vacuo, giving crude product that was purified by column chromatography over silica eluting with chloroform/methanol (95:5), yielding 0.41 g (44%) of a colorless oil. ^{1}H NMR (CDCl₃) δ 7.52 (s, 1H), 7.12 (m, 2H), 7.08 (s, 1H), 7.03 (m, 2H), 6.87 (s, 1H), 5.08 (s, 2H). GC-MS: *m/z* = 176 (molecular ion). LC-MS: *m/z* = 177 (M + 1).

1-(4-Cyanobenzyl)-1*H*-imidazole (1b). Using 4-cyanobenzyl bromide **10b**, sodium carbonate as base and chloroform as the solvent. The crude product was dissolved in 1 M aqueous hydrochloride and washed twice with ether. After bringing the

pH to 10, the aqueous solution was extracted with chloroform, after which the organic layer was dried over Na_2SO_4 and evaporated to dryness, yielding 3.96 g (42%) of a white solid. ^{1}H NMR (DMSO-d_6) δ 7.85 (d, 2H, J = 8.4), 7.79 (s, 1H), 7.38 (d, 2H, J = 8.4), 7.22 (s, 1H), 6.95 (s, 1H), 5.32 (s, 2H). LC-MS: m/z = 184 (M + 1).

1-(4-Chlorobenzyl)-1*H*-imidazole (1d). Using 4-chlorobenzylchloride **10d**. Purification was performed by column chromatography on silica eluting with chloroform/methanol (95:5) to give 0.81 g (68%) of product. ^{1}H NMR (CDCl$_3$) δ 7.52 (s, 1H), 7.32 (d, 2H, J = 8.4), 7.09 (s, 1H), 7.06 (d, 2H, J = 8.4), 6.87 (s, 1H), 5.08 (s, 2H). LC-MS: m/z = 193 (M + 1). GC-MS: m/z = 192 (molecular ion).

1-(4-Bromobenzyl)-1*H*-imidazole (1e). Using 4-bromobenzylbromide **10e**. Purification was performed by column chromatography on silica eluting with chloroform/methanol (95:5–90:10) to give 0.42 g (44%) of a slightly yellow solid. ^{1}H NMR (CDCl$_3$) δ 7.54 (s, 1H), 7.43 (d, 2H, J = 8.4), 7.10 (s, 1H), 7.02 (d, 2H, J = 8.4), 6.88 (s, 1H), 5.08 (s, 2H). LC-MS: m/z = 237 (M + 1).

1-(4-Aminobenzyl)-1*H*-imidazole (1g). 4-Nitrobenzyl bromide **10i** and imidazole were reacted in refluxing acetone, applying potassium carbonate as base. Purification was performed by column chromatography on silica eluting with chloroform/methanol (97.5:2.5–95:5) to give 1.97 g (42%) of a white solid, the nitro precursor. ^{1}H NMR (CDCl$_3$) δ 8.19 (d, 2H, J = 8.4), 7.58 (s, 1H), 7.24 (d, 2H, J = 8.4), 7.13 (s, 1H), 6.88 (s, 1H), 5.33 (s, 2H). LC-MS: m/z = 204 (M + 1). 1-(4-Nitrobenzyl)-1*H*-imidazole (0.5 g, 2.5 mmol) was weighed in a high pressure vessel and dissolved in 2.5 mL of ethanol, 2.5 mL of ethyl acetate, and 1 mL of a 1 M aqueous hydrochloride solution. The mixture was purged with argon, and Pd/C (10%, 0.05 g) was then added. The mixture was shaken in a Parr apparatus at 40 psi H_2 pressure. After 30 min, the mixture was filtered over celite and the filtrate was concentrated and divided between chloroform (10 mL) and a saturated sodium bicarbonate solution (10 mL). The aqueous layer was extracted with chloroform (10 mL), and the combined organic layers were washed with water, dried over Na_2SO_4, and evaporated in vacuo to dryness yielding 0.32 g (75%) of a white solid. ^{1}H NMR (CDCl$_3$) δ 7.49 (s, 1H), 7.04 (s, 1H), 6.97 (d, 2H, J = 8.4), 6.87 (s, 1H), 6.64 (d, 2H, J = 8.4), 4.96 (s, 2H), 3.75 (bs, 2H). LC-MS: m/z = 174 (M + 1).

1-(3-Cyanobenzyl)-1*H*-imidazole (2b). Using 3-cyanobenzyl bromide **10j**. Purification was performed by column chromatography on silica eluting with chloroform/methanol (95:5) to give 0.43 g (46%) of product. ^{1}H NMR (CDCl$_3$) δ 7.63 (d, 1H, J = 7.7), 7.57 (s, 1H), 7.49 (t, 1H, J = 7.7), 7.43 (s, 1H), 7.36 (d, 1H, J = 7.7), 7.14 (s, 1H), 6.91 (s, 1H), 5.18 (s, 2H). LC-MS: m/z = 184 (M + 1). GC-MS: m/z = 183 (molecular ion).

1-(3-Fluorobenzyl)-1*H*-imidazole (2c). Using 3-fluorobenzyl bromide **10k**. Purification was performed by column chromatography on silica eluting with chloroform/methanol (95:5) to give 0.46 g (49%) of product. ^{1}H NMR (CDCl$_3$) δ 7.55 (s, 1H), 7.32 (m, 1H), 7.11 (s, 1H), 7.01 (m, 1H), 6.93 (d, 1H, J = 7.3), 6.90 (s, 1H), 6.83 (d, 1H, J = 9.1), 5.12 (s, 2H). LC-MS: m/z = 177 (M + 1). GC-MS: m/z = 176 (molecular ion).

1-(3-Chlorobenzyl)-1*H*-imidazole (2d). Using 3-chlorobenzyl bromide **10l**. Purification was performed by column chromatography on silica eluting with chloroform/methanol (95:5) to give 0.30 g (32%) of product. ^{1}H NMR (CDCl$_3$) δ 7.54 (s, 1H), 7.29 (m, 2H), 7.12 (m, 2H), 7.01 (m, 1H), 6.89 (t, 1H, J = 1.8), 5.09 (s, 2H). LC-MS: m/z = 193 (M + 1). GC-MS: m/z = 192 (molecular ion).

1-(3-Bromobenzyl)-1*H*-imidazole (2e). Using 3-bromobenzylbromide **10m**. Purification was performed by column chromatography on silica eluting with chloroform/methanol (95:5) to give 0.42 g (44%) of product. ^{1}H NMR (CDCl$_3$) δ 7.55 (s, 1H), 7.46 (d, 1H, J = 8.1), 7.30 (s, 1H), 7.23 (t, 1H, J = 7.7), 7.11 (s, 1H), 7.07 (m, 1H), 6.90 (t, 1H, J = 1.2), 5.09 (s, 2H). LC-MS: m/z = 239 (M + 1). GC-MS: m/z = 236 and 238 (molecular ions).

The series of imidazoles **3** were prepared using a similar procedure as that for compound **3b**. Details and changes with respect to the procedure for **3b** are given below.

Methyl 3-[1-(4-Cyanobenzyl)-1*H*-imidazol-5-yl]-propanoate (3b). Methyl 3-(1-trityl-1*H*-imidazol-4-yl)-propanoate **14** (1.0 g, 2.5 mmol) and 4-cyanobenzyl bromide **10b** (0.5 g, 2.5 mmol) were dissolved in 10 mL of acetonitrile and stirred overnight at 80 °C. The mixture was concentrated and triturated using 10 mL of ethyl acetate. The precipitate was collected by filtration and washed with ethyl acetate. The solids were refluxed for 30 min in 20 mL of methanol. The resulting solution was evaporated in vacuo and triturated with 10 mL of ethyl acetate. After washing with ethyl acetate, the solid was taken up in a saturated NaHCO$_3$ solution (15 mL), and this solution was extracted twice with 15 mL of chloroform. The combined organic layers were washed with a saturated NaHCO$_3$ solution, dried over Na_2SO_4, and evaporated to dryness, giving a yellowish oil that was purified by column chromatography on silica gel eluting with CHCl$_3$/MeOH (95:5–90:10) resulting in 0.51 g (75%) of a slightly yellow solid. ^{1}H NMR (CDCl$_3$) δ 7.65 (d, 2H, J = 8.4), 7.51 (s, 1H), 7.13 (d, 2H, J = 8.4), 6.89 (s, 1H), 5.19 (s, 2H), 3.66 (s, 3H), 2.69 (t, 2H, J = 7.7), 2.60 (t, 2H, J = 7.7). LC-MS: m/z = 270 (M + 1).

Methyl 3-(1-Benzyl-1*H*-imidazol-5-yl)-propanoate (3a). Using **14** and benzyl bromide **10a** and applying a reaction temperature of 65 °C. Purification by column chromatography on silica gel eluting with chloroform/methanol (95:5) resulting in 1.18 g (64%) of a white solid. ^{1}H NMR (CDCl$_3$) δ 7.48 (s, 1H), 7.34 (m, 3H), 7.05 (d, 2H, J = 7.3), 6.85 (s, 1H), 5.09 (s, 2H), 3.65 (s, 3H), 2.75 (t, 2H, J = 7.7), 2.56 (t, 2H, J = 7.7). LC-MS: m/z = 245 (M + 1).

Methyl 3-[1-(4-Fluorobenzyl)-1*H*-imidazol-5-yl]-propanoate (3c). Using **14** and 4-fluorobenzyl bromide **10c**. Purification was performed by column chromatography on silica gel eluting with chloroform/methanol (95:5) resulting in 0.51 g (77%) of a white solid. ^{1}H NMR (CDCl$_3$) δ 7.47 (d, 1H, J = 1.1), 7.04 (s, 2H), 7.03 (s, 2H), 6.85 (s, 1H), 5.08 (s, 2H), 3.67 (s, 3H), 2.74 (t, 2H, J = 7.5), 2.57 (t, 2H, J = 7.5). GC-MS: m/z = 262 (molecular ion).

Methyl 3-[1-(4-Chlorobenzyl)-1*H*-imidazol-5-yl]-propanoate (3d). Using **14** and 4-chorobenzyl chloride **10d**. Purification by column chromatography on silica gel eluting with chloroform/methanol (99:1–98:2) resulting in 0.09 g (13%) of a colorless oil. ^{1}H NMR (CDCl$_3$) δ 7.48 (s, 1H), 7.32 (d, 2H, J = 8.4), 6.99 (d, 2H, J = 8.4), 6.85 (s, 1H), 5.08 (s, 2H), 3.67 (s, 3H), 2.72 (t, 2H, J = 7.5), 2.59 (t, 2H, J = 7.5). GC-MS: m/z = 278, 280 (molecular ions).

Methyl 3-[1-(4-Bromobenzyl)-1*H*-imidazol-5-yl]-propanoate (3e). Using **14** and 4-bromobenzyl bromide **10e**. Purification was performed by column chromatography on silica gel eluting with chloroform/methanol (95:5) resulting in 0.49 g (60%) of a white solid. ^{1}H NMR (CDCl$_3$) δ 7.48 (s, 1H), 7.47 (d, 2H, J = 8.6), 6.92 (d, 2H, J = 8.6), 6.85 (s, 1H) 5.06 (s, 2H), 3.67 (s, 3H), 2.72 (t, 2H, J = 8.0), 2.58 (t, 2H, J = 8.0). LC-MS: m/z = 325 (M + 1).

Methyl 3-[1-(4-Methoxybenzyl)-1*H*-imidazol-5-yl]-propanoate (3h). Using **14** and 4-methoxybenzyl bromide **10h** and applying a reaction temperature of 55 °C. Purified by column chromatography on silica gel eluting with chloroform/methanol (100:0–95:5) resulting in 0.49 g (71%) of a slightly yellow solid. ^{1}H NMR (CDCl$_3$) δ 7.45 (s, 1H), 7.00 (d, 2H, J = 8.4), 6.86 (d, 2H, J = 8.4), 6.82 (s, 1H), 5.01 (s, 2H), 3.79 (s, 3H), 3.66 (s, 3H), 2.76 (t, 2H, J = 7.5), 2.56 (t, 2H, J = 7.5). LC-MS: m/z = 275 (M + 1).

The series of imidazoles **4b–4e** were prepared using a similar procedure as that for compound **4b**, while **4a** was prepared in a similar way as **4h**.

3-(1-Benzyl-1*H*-imidazol-5-yl)-1-propanol (4a). Using a similar procedure as that for **4h** starting with methyl 3-(1-benzyl-1*H*-imidazol-5-yl)-propanoate **3a** yielding 0.44 g (57%) of a

colorless oil. ¹H NMR (CDCl₃) δ 7.40 (s, 1H), 7.29 (m, 3H), 7.03 (d, 2H, *J* = 7.7), 6.79 (s, 1H), 5.04 (s, 2H), 3.95 (bs, 1H), 3.61 (t, 2H, *J* = 6.3), 2.52 (t, 2H, *J* = 7.5), 1.79 (m, 2H). LC-MS: *m/z* = 217 (M + 1).

3-[1-(4-Cyanobenzyl)-1*H*-imidazol-5-yl]-1-propanol (4b). A solution of 4-(3-((trimethylsilyl)oxy)propyl)-1-trityl-1*H*-imidazole **16** (19.8 g, 45 mmol) and 4-cyanobenzyl bromide **10b** (8.8 g, 45 mmol) in 250 mL of acetonitrile was refluxed overnight. The solution was concentrated and dissolved in a mixture of 80 mL of acetic acid and 20 mL of water, and this mixture was refluxed until a white solid precipitated. Water (200 mL) was added, and after cooling down to room temperature the mixture was extracted twice with diethyl ether. The aqueous phase was adjusted to pH 9 with a 4 M NaOH solution and was then extracted with methylene chloride. The organic extracts were dried over Na₂SO₄ and evaporated to give a slightly yellow solid. Trituration with cold acetone yielded 6.5 g (59%) of a white solid. ¹H NMR (CDCl₃) δ 7.62 (d, 2H, *J* = 8.6), 7.48 (s, 1H), 7.12 (d, 2H, *J* = 8.6), 6.87 (s, 1H), 5.17 (s, 2H), 3.65 (t, 2H, *J* = 6.1), 2.69 (bs, 1H), 2.52 (t, 2H, *J* = 7.7), 1.84 (m, 2H). ¹³C NMR (CDCl₃) δ 141.8, 137.4, 132.8, 131.6, 127.0, 126.9, 118.3, 112.0, 61.2, 47.8, 31.0, 20.1. LC-MS: *m/z* = 242 (M + 1).

3-[1-(4-Fluorobenzyl)-1*H*-imidazol-5-yl]-1-propanol (4c). Using **16** and 4-fluorobenzyl bromide **10c**. Purification was performed by column chromatography on silica gel eluting with chloroform/methanol (95:5–90:10) to give 0.3 g (55%) of a white solid. ¹H NMR (CDCl₃) δ 7.46 (s, 1H), 7.04 (s, 2H), 7.02 (s, 2H), 6.86 (s, 1H), 5.05 (s, 2H), 3.66 (t, 2H, *J* = 6.1), 2.53 (t, 2H, *J* = 7.3), 1.82 (m, 2H), 1.65 (bs, 1H). LC-MS: *m/z* = 235 (M + 1).

3-[1-(4-Chlorobenzyl)-1*H*-imidazol-5-yl]-1-propanol (4d). Using **16** and 4-chlorobenzyl chloride **10d**. Purification was performed by column chromatography on silica gel eluting with chloroform/methanol (95:5–90:10) to give 0.2 g (25%) of a white solid. ¹H NMR (CDCl₃) δ 7.44 (s, 1H), 7.29 (d, 2H, *J* = 8.4), 6,96 (d, 2H, *J* = 8.4), 6.83 (s, 1H), 5.04 (s, 2H), 3.65 (t, 2H), 2.51 (t, 2H, *J* = 7.5), 2.25 (bs, 1H), 1.81 (m, 2H). LC-MS: *m/z* = 251 (M + 1).

3-[1-(4-Bromobenzyl)-1*H*-imidazol-5-yl]-1-propanol (4e). Using **16** and 4-bromobenzyl bromide **10e**. Purification was performed by column chromatography on alumina eluting with chloroform/methanol (99:1–95:5) to give 0.7 g (52%) of a white solid. ¹H NMR (CDCl₃) δ 7.47 (s, 1H), 7.46 (d, 2H, *J* = 8.2), 6.90 (d, 2H, *J* = 8.2), 6.85 (s, 1H), 5.03 (s, 2H), 3.66 (t, 2H, *J* = 6.2), 2.50 (t, 2H, *J* = 7.7), 2.1 (bs, 1H), 1.82 (m, 2H). LC-MS: *m/z* = 297 (M + 1).

3-[1-(4-Methoxybenzyl)-1*H*-imidazol-5-yl]-1-propanol (4h). A solution of methyl 3-[1-(4-methoxybenzyl)-1*H*-imidazol-5-yl]-propanoate **3h** (0.48 g, 1.76 mmol) in 3.5 mL of freshly distilled THF was added dropwise (carefully) to an ice-cooled suspension of lithium aluminiumhydride (0.1 g, 2.64 mmol) in 1.5 mL of freshly distilled THF. After stirring for 2 h, the reaction mixture was quenched by carefully adding 1.5 mL of a 0.1 M aqueous solution of NaOH. The resulting suspension was filtered and washed with THF, after which the filtrate was concentrated and dissolved in 10 mL of dichloromethane. The dichloromethane solution was washed twice with 10 mL of a 0.1 M aqueous solution of NaOH, dried over Na₂SO₄, and evaporated to dryness, giving 0.36 g (83%) of a colorless oil. ¹H NMR (CDCl₃) δ 7.43 (s, 2H), 6.99 (d, 2H, *J* = 8.6), 6.85 (d, 2H, *J* = 8.6), 6.82 (s, 1H), 4.99 (s, 2H), 3.79 (s, 3H), 3.65 (t, 2H, *J* = 6.2), 2.55 (t, 2H, *J* = 7.5), 2.18 (bs, 1H), 1.81 (m, 2H). LC-MS: *m/z* = 247 (M + 1).

The series of imidazoles **5** and **6** have been prepared using a similar procedure as that for compound **5c**. Details and changes with respect to the procedure for **5c** are given below.

1-(4-Fluorobenzyl)-5-phenyl-1*H*-imidazole (5c). A solution of 4-phenyl-1-trityl-1*H*-imidazole **9g** (0.25 g, 0.65 mmol) and 4-fluorobenzyl bromide **10c** (0.12 g, 0.65 mmol) in 2 mL of acetonitrile and 0.5 mL of chloroform was stirred overnight at 80 °C. The solution was concentrated and dissolved in a mixture of 1.25 mL of acetic acid and 1 mL of water, and this mixture was refluxed until a white solid precipitated. A 1 M HCl solution

(7.5 mL) was added, and after cooling down to room temperature, the mixture was extracted twice with 5 mL portions of diethyl ether. The organic phase was extracted with 7.5 mL of a 1 M solution of HCl. The combined aqueous phases were adjusted to pH 8 with a 6 M NaOH solution and were then extracted twice with 10 mL portions of methylene chloride. The methylene chloride extracts were dried over Na₂SO₄ and evaporated in vacuo to give a slightly yellow oil. This crude product was purified by column chromatography using silica gel and eluting with a chloroform/methanol gradient yielding 60 mg (37%) of a colorless oil. ¹H NMR (CDCl₃) δ 7.56 (s, 1H), 7.36 (m, 3H), 7.27 (m, 2H), 7.13 (s, 1H), 6.97 (m, 4H), 5.12 (s, 2H). LC-MS: *m/z* = 253 (M + 1).

1-Benzyl-5-phenyl-1*H*-imidazole (5a). Using **9g** and benzyl bromide **10a** yielding 93 mg (61%) of a white solid. ¹H NMR (CDCl₃) δ 7.55 (d, 1H, *J* = 0.8), 7.29 (m, 8H), 7.14 (s, 1H), 7.01 (d, 2H, *J* = 8.0), 5.14 (s, 2H). LC-MS: *m/z* = 235 (M + 1). GC-MS: *m/z* = 234 (molecular ion).

1-(4-Cyanobenzyl)-5-phenyl-1*H*-imidazole (5b). Using **9g** and 4-cyanobenzyl bromide **10b** yielding 5.5 g (68%) of white solid. ¹H NMR (CDCl₃) δ 7.61 (s, 1H), 7.58 (d, 2H, *J* = 8.4), 7.36 (m, 3H), 7.22 (m, 2H), 7.17 (s, 1H), 7.06 (d, 2H, *J* = 8.4), 5.23 (s, 2H). ¹³C NMR δ 142.1, 138.6, 133.4, 132.7, 129.2, 128.8, 128.4, 127.1, 118.3, 112.0, 48.3. LC-MS: *m/z* = 260 (M + 1). GC-MS: *m/z* = 259 (molecular ion).

1-(4-Chlorobenzyl)-5-phenyl-1*H*-imidazole (5d). Using **9g** and 4-chlorobenzyl chloride **10d**. For speeding up the reaction, ca. 1 mol equiv of NaI was added to the reaction mixture to in situ convert the benzyl chloride to the benzyl iodide. Purification yielded 21 mg (12%) of a yellowish oil. ¹H NMR (CDCl₃) δ 7.57 (s, 1H), 7.36 (m, 3H), 7.26 (m, 4H), 7.14 (s, 1H), 6.92 (d, 2H, *J* = 8.8), 5.12 (s, 2H). LC-MS: *m/z* = 269 and 271 (M + 1 isotopic ions).

1-(4-Bromobenzyl)-5-phenyl-1*H*-imidazole (5e). Using **9g** and 4-bromobenzyl bromide **10e** yielding 79 mg (39%) of a slightly yellow solid. ¹H NMR (CDCl₃) δ 7.57 (d, 1H, *J* = 0.9), 7.42 (d, 2H, *J* = 8.4), 7.36 (m, 3H), 7.26 (m, 2H), 7.15 (d, 1H, *J* = 0.9), 6.87 (d, 2H, *J* = 8.4), 5.11 (s, 2H). LC-MS: *m/z* = 315 (M + 1).

1-(4-Methoxybenzyl)-5-phenyl-1*H*-imidazole (5h). Using **9g** and 4-methoxybenzyl bromide **10h** yielding 96 mg (56%) of an oil. ¹H NMR (CDCl₃) δ 7.52 (s, 1H), 7.32 (m, 5H), 7.12 (s, 1H), 6.94 (d, 2H, *J* = 8.6), 6.82 (d, 2H, *J* = 8.6), 5.06 (s, 2H), 3.76 (s, 3H). LC-MS: *m/z* = 265 (M + 1).

1-(4-Cyanobenzyl)-5-(methylene-acetate)-1*H*-imidazole (6a). This compound was made starting from commercially available 4-(hydroxymethyl)-imidazole **8f** following the literature procedure of Millet et al.,[37] involving subsequent tritylation, acetylation, alkylation with 4-cyanobenzyl bromide **10b**, and deprotection of the trityl group. Yield: 0.87 g (65%) of a white solid. ¹H NMR (CDCl₃) δ 7.65 (d, 2H, *J* = 8.2), 7.58 (s, 1H), 7.20 (s, 1H), 7.14 (d, 2H, *J* = 8.2), 5.26 (s, 2H), 4.97 (s, 2H), 1.85 (s, 3H). LC-MS: *m/z* = 256 (M + 1).

1-(4-Cyanobenzyl)-5-(methyl carboxylate)-1*H*-imidazole (6b). Using methyl 1-trityl-1*H*-imidazole-4-carboxylate **9b** and 4-cyanobenzyl bromide **10b** yielding 27 mg (11%) of a white solid. ¹H NMR (CDCl₃) δ 7.80 (s, 1H), 7.71 (s, 1H), 7.63 (d, 2H, *J* = 8.3), 7.22 (d, 2H, *J* = 8.3), 5.59 (s, 2H), 3.80 (s, 3H). LC-MS: *m/z* = 242 (M + 1).

1-(4-Cyanobenzyl)-5-methyl-1*H*-imidazole (6c). Using 4-methyl-1-trityl-1*H*-imidazole **9c** and 4- cyanobenzyl bromide **10b** yielding 0.71 g (78%) of a slightly yellow solid. ¹H NMR (CDCl₃) δ 7.64 (d, 2H, *J* = 8.4), 7.50 (s, 1H), 7.12 (d, 2H, *J* = 8.4), 6.87 (s, 1H), 5.14 (s, 2H), 2.07 (s, 3H). LC-MS: *m/z* = 198 (M + 1). GC-MS: *m/z* = 197 (molecular ion).

1-(4-Cyanobenzyl)-5-bromo-1*H*-imidazole (6d). Using 4-bromo-1-trityl-1*H*-imidazole **9d** and 4- cyanobenzyl bromide **10b** yielding 84 mg (31%) of a white solid. ¹H NMR (CDCl₃) δ 7.64 (d, 2H, *J* = 8.4), 7.63 (s, 1H), 7.19 (d, 2H, *J* = 8.4), 7.10 (s, 1H), 5.20 (s, 2H). LC-MS: *m/z* = 262 (M + 1). GC-MS: *m/z* = 261 and 263 (ionic isotopes).

1-(4-Cyanobenzyl)-5-formyl-1*H*-imidazole (6e). Using 4-formyl-1-trityl-1*H*-imidazole **9e** and 4-cyanobenzyl bromide **10b** yielding 57 mg (37%) of a slightly yellow solid. ^{1}H NMR (CDCl$_3$) δ 9.74 (s, 1H), 7.88 (s, 1H), 7.79 (s, 1H), 7.63 (d, 2H, J = 8.5), 7.26 (d, 2H, J = 8.5), 5.58 (s, 2H). LC-MS: m/z = 212 (M + 1).

1-(4-Cyanobenzyl)-5-hydroxymethyl-1*H*-imidazole (6f). This compound was prepared by hydrolysis of **6a**, as described by Millet et al.[37] Yield: 0.3 g (72%) of a white solid. ^{1}H NMR (DMSO-d_6) δ 7.83 (d, 2H, J = 8.2), 7.72 (s, 1H), 7.30 (d, 2H, J = 8.2), 6.86 (s, 1H), 5.35 (s, 2H), 5.12 (t, 1H, J = 5.2), 4.30 (d, 2H, J = 5.2). LC-MS: m/z = 214 (M + 1).

1-(4-Cyanobenzyl)-5-(4-pyridyl)-1*H*-imidazole (6g). 1-(4-Cyanobenzyl)-5-bromo-1*H*-imidazole **6d** (100 mg, 0.38 mmol), 4-pyridinyl boronic acid **17h** (52 mg, 0.42 mmol), 0.38 mL of a 2 M aqueous solution of K$_3$PO$_4$ (0.76 mmol), and 1 mL of DMF were weighed in a Schlenck tube and capped with a rubber septum. Three cycles of freeze−pump−thaw were performed to remove the oxygen from the reaction mixture, and tetrakis-(triphenylphosphine)palladium(0) (18 mg, 15 μmol) was added. The reaction mixture was then stirred overnight at 85 °C. To the reaction mixture were added 3 mL of ethyl acetate and 6 mL of water. After stirring a few moments, the layers were separated and the water layer was extracted with ethyl acetate. The combined organic layers were dried over MgSO$_4$, and the solvent was evaporated in vacuo, giving crude product that was purified by column chromatography over silica eluting with ethyl acetate/hexane/methanol (2:1:0−96:0:4) and a second column eluting with chloroform/methanol (95:5) yielding 58 mg (58%) of product. ^{1}H NMR (CDCl$_3$) δ 8.57 (d, 2H, J = 6.0), 7.66 (s, 1H), 7.60 (d, 2H, J = 8.1), 7.33 (s, 1H), 7.13 (d, 2H, J = 6.0), 7.09 (d, 2H, J = 8.1), 5.31 (s, 2H). LC-MS: m/z = 261 (M + 1). GC-MS: m/z = 260 (molecular ion).

The imidazole series **7** were prepared using a similar procedure as that for compound **7b**.

1-(4-Cyanobenzyl)-5-(2-methylphenyl)-1*H*-imidazole (7b). 1-(4-Cyanobenzyl)-5-bromo-1*H*-imidazole **6d** (80 mg, 0.31 mmol), 2-methylphenyl boronic acid **17b** (46 mg, 0.34 mmol), and Na$_2$CO$_3$ (0.76 mmol) were weighed in a Schlenck tube, capped with a rubber septum. The reaction tube was filled with argon and subsequently with 1.5 mL of a 1:1:1 mixture of water, dimethoxy ethane, and ethanol. The mixture was heated to 75 °C upon which a clear solution developed. Three cycles of freeze−pump−thaw were performed to remove the oxygen from the reaction mixture, and tetrakis(triphenylphosphine)palladium(0) (0.7 mg, 0.6 μmol) was added. The reaction mixture was then stirred overnight at 75 °C. The mixture was concentrated, 2.5 mL of chloroform was added, and the mixture was washed twice with 2 mL portions of a saturated NaHCO$_3$ solution. The organic layer was dried over Na$_2$SO$_4$, and the solvent was evaporated in vacuo, giving crude product that was purified by column chromatography over silica eluting with chloroform/methanol (98:2) and a second column eluting with ethyl acetate/hexane (1:1−4:1), yielding 46 mg (55%) of a colorless oil. ^{1}H NMR (CDCl$_3$) δ 7.67 (s, 1H), 7.51 (d, 2H, J = 8.3), 7.3−7.1 (m, 3H), 7.04 (m, 2H), 6.95 (d, 2H, J = 8.3), 4.98 (s, 2H), 2.02 (s, 3H). LC-MS: m/z = 274 (M + 1).

1-(4-Cyanobenzyl)-5-(2-fluorophenyl)-1*H*-imidazole (7a). Using 2-fluorophenyl boronic acid **17a** and purifying by column chromatography over silica eluting with ethyl acetate/hexane (1:1−4:1) yielded 32 mg (38%) of a slightly yellow solid. ^{1}H NMR (CDCl$_3$) δ 7.63 (s, 1H), 7.53 (d, 2H, J = 8.4), 7.36 (m, 1H), 7.14 (m, 4H), 7.04 (d, 2H, J = 8.4), 5.15 (s, 2H). LC-MS: m/z = 278 (M + 1).

1-(4-Cyanobenzyl)-5-(3-fluorophenyl)-1*H*-imidazole (7c). Using 3-fluorophenyl boronic acid **17c** and purifying by column chromatography over silica eluting with ethyl acetate/hexane (2:1−4:1) yielded 52 mg (61%) of a white solid. ^{1}H NMR (CDCl$_3$) δ 7.63 (s, 1H), 7.60 (d, 2H, J = 8.4), 7.32 (m, 1H), 7.19 (s, 1H), 7.08 (d, 2H, J = 8.4), 7.02 (m, 2H), 6.94 (m, 1H), 5.26 (s, 2H). LC-MS: m/z = 278 (M + 1).

1-(4-Cyanobenzyl)-5-(3-methylphenyl)-1*H*-imidazole (7d). Using 3-methylphenylboronic acid **17d** and purifying by column

chromatography over silica eluting with chloroform/methanol (98:2) and a second column eluting with ethyl acetate/hexane (1:1−4:1) yielded 29 mg (35%) of a white solid. ^{1}H NMR (CDCl$_3$) δ 7.60 (s, 1H), 7.59 (d, 2H, J = 8.4), 7.25−6.95 (m, 7H), 5.22 (s, 2H), 2.32 (s, 3H). LC-MS: m/z = 274 (M + 1).

1-(4-Cyanobenzyl)-5-(4-fluorophenyl)-1*H*-imidazole (7e). Using 4-fluorophenyl boronic acid **17e** and purifying by column chromatography over silica eluting with chloroform/methanol (99:1−98:2) yielded 75 mg (89%) of a white solid. ^{1}H NMR (CDCl$_3$) δ 7.64 (s, 1H), 7.58 (d, 2H, J = 8.0), 7.18 (m, 2H), 7.14 (s, 1H), 7.05 (m, 4H), 5.20 (s, 2H). LC-MS: m/z = 278 (M + 1).

1-(4-Cyanobenzyl)-5-(4-methylphenyl)-1*H*-imidazole (7f). Using 4-methylphenyl boronic acid **17f** and purifying by column chromatography over silica eluting with chloroform/methanol (99:1−98:2) yielded 37 mg (71%) of a white solid. ^{1}H NMR (CDCl$_3$) δ 7.60 (s, 1H), 7.58 (d, 2H, J = 8.1), 7.2−7.0 (m, 7H), 5.21 (s, 2H), 2.36 (s, 3H). LC-MS: m/z = 274 (M + 1). GC-MS: m/z = 273 (molecular ion).

The tritylated imidazole building blocks **9** were prepared as described below for **9c**, unless indicated otherwise.

4-Methyl-1-trityl-1*H*-imidazole (9c). A solution of 4-methyl-1*H*-imidazole **8c** (0.99 g, 12 mmol) and triethyl amine (3.4 g, 34 mmol) in 15 mL of chloroform was added to an ice-cooled solution of trityl chloride (3.7 g, 13 mmol) in 15 mL of chloroform. The reaction mixture was stirred for 1 h at ambient temperature and was then washed twice with 15 mL portions of a 0.5 M HCl solution and once with 15 mL of a saturated NaHCO$_3$ solution. The organic layer was dried over Na$_2$SO$_4$ and evaporated in vacuo. The resulting solid was triturated with 15 mL of diethyl ether, filtered, and washed with diethyl ether yielding 3.7 g (93%) of a white solid. ^{1}H NMR (CDCl$_3$) δ 7.32 (m, 10H), 7.15 (m, 6H), 6.51 (s, 1H), 2.10 (s, 3H). LC-MS: m/z = 325 (M + 1) and 243 (trityl radical cation). GC-MS: m/z = 243 (trityl radical cation), the molecular ion is not observed.

4-(Methylene acetate)-1-trityl-1*H*-imidazole (9a). This compound was made by acylation of **9f** following the procedure of Millet et al.[37]

Methyl 1-Trityl-1*H*-imidazole-4-carboxylate (9b). A few ml of *N,N*-dimethylformamide (DMF) was used as cosolvent to dissolve the starting compound methyl 1*H*-imidazole-4-carboxylate **8b**. The DMF was removed by trituration with water, followed by trituration with diethyl ether to yield 0.4 g (56%) of a white solid. ^{1}H NMR (CDCl$_3$) δ 7.59 (s, 1H), 7.62 (s, 1H), 7.35 (m, 9H), 7.12 (m, 6H), 3.85 (s, 3H). LC-MS: m/z = 737 (2M+1) and 243 (trityl radical cation). GC-MS: m/z = 243 (trityl radical cation).

4-Bromo-1-trityl-1*H*-imidazole (9d). Using 4-bromo-1*H*-imidazole **8d** yielding 0.77 g (73%) of a white solid. ^{1}H NMR (CDCl$_3$) δ 7.35 (m, 9H), 7.30 (s, 1H), 7.10 (m, 6H), 6.80 (s, 1H). LC-MS: m/z = 391 (M + 1) and 243 (trityl radical cation). GC-MS: m/z = 243 (trityl radical cation).

4-Formyl-1-trityl-1*H*-imidazole (9e). A few mL of *N,N*-dimethylformamide (DMF) were used as cosolvent to dissolve the starting compound 1*H*-imidazole-4-carbaldehyde **8e**. The DMF was removed by trituration with water, followed by trituration with diethyl ether to yield 0.6 g (69%) of a white solid. ^{1}H NMR (CDCl$_3$) δ 9.85 (s, 1H), 7.61 (s, 1H), 7.52 (s, 1H), 7.35 (m, 9H), 7.10 (m, 6H). LC-MS: m/z = 677 (2M + 1) and 243 (trityl radical cation). GC-MS: m/z = 243 (trityl radical cation).

4-(Hydroxymethyl)-1-trityl-1*H*-imidazole (9f). This compound was made by tritylation of commercially available 4-(hydroxymethyl)-imidazole **8f** following the procedure of Millet et al.[37]

4-Phenyl-1-trityl-1*H*-imidazole (9g). Using 4-phenyl-1*H*-imidazole **8g** yielding 2.4 g (90%) of a white solid. ^{1}H NMR (CDCl$_3$) δ 7.7 (d, 2H, J = 8.4), 7.48 (s, 1H), 7.32 (m 11H), 7.20 (m, 7H), 7.10 (m, 1H). LC-MS: m/z = 387 (M + 1) and 243 (trityl radical cation). GC-MS: m/z = 386 (molecular ion) and 243 (trityl radical cation).

Methyl 3-(1-Trityl-1*H*-imidazol-4-yl)-propanoate (14). This precursor was synthesized starting with urocanic acid **11** by following the literature procedure of Stark et al.[33]

4-(3-((Trimethylsilyl)oxy)propyl)-1-trityl-1*H*-imidazole (16). A solution of trimethylsilyl chloride (36.0 g, 331 mmol) in 200 mL of chloroform was added dropwise to an ice-cooled solution of 3-(1-(trityl)-1*H*-imidazol-4-yl)propanol **15**[33] (101.8 g, 276 mmol) and triethylamine (39.0 g, 386 mmol) in 600 mL of chloroform. After stirring for 1 h, the solution was concentrated and diluted with 600 mL of diethyl ether, giving a white precipitate. The precipitate was collected by filtration and washed with 600 mL of diethyl ether. Concentration of the filtrate and coevaporation with diethyl ether yielded a quantitative yield of a slightly yellow solid. ^{1}H NMR (CDCl$_3$) δ 7.35 (m, 10H), 7.15 (m, 6H), 6.55 (s, 1H), 3.61 (t, 2H, $J = 6.2$), 2.60 (t, 2H, $J = 7.5$), 1.85 (m, 2H), 0.10 (s, 9H). LC-MS: $m/z = 369$ and 243 for the TMS-deprotected H$^+$-species and the trityl radical cation, the $(M + 1)^+$ species is not observed. GC-MS: $m/z = 243$ (trityl radical cation), the molecular ion is not observed.

Biological Assays (Inhibition of CYP11B1 and CYP11B2). Inhibitor potencies for human CYP11B1 and CYP11B2 were determined in an in vitro assay using V79 cells in which the human CYP11B1 or CYP11B2 are stably (over)expressed. The human CYP11B1 (over)expressing V79 cells (stably transfected with a pcDNA3.1 vector, carrying a hygromycin resistance box) were constructed at Organon (Newhouse, UK) as described in Roumen et al.[29] The V79 cells stably (over)expressing human CYP11B2 were developed in the laboratory of Prof. Rita Bernhardt, Institute of Biochemistry, Saarland University, Saarbrücken, Germany.[34−36]

Cells were cultured under standard conditions in DMEM/FK12 medium (Gibco, Gaithersburg, MD) supplemented with 10% fetal calf serum (Hyclone, Logan, UT), penicillin/streptomycin (100 U/mL and 100 μg/mL, respectively, both from Gibco). Cell culturing and incubation experiments with the cells were performed at 37 °C in a humid environment and 5% CO$_2$ atmosphere.

For assessing inhibitor potencies, cells were transferred to 12-well plates and grown until they were confluent. Next, cells were incubated for 1 h in serum free medium with cumulative inhibitor concentrations. Subsequently, 11-deoxycorticosterone (Sigma-Aldrich, St Louis, MO) was added as substrate to obtain a final concentration of 500 nM ($0.5 \times$ Km), following incubation of the plates for another hour for V79 CYP11B1 or another 3 h for V79 CYP11B2. After these incubation times, medium was collected for steroid analysis by HPLC. To extract the (produced) steroids from the medium, 1 mL aliquots of medium were mixed with 1 mL of 1 M sodium-glycine buffer (pH 10.5) containing 500 nM methylprednisolone (Sigma-Aldrich) as internal standard and 5 mL of diethylether (Biosolve, Valkenswaard, The Netherlands). After shaking for 3 min, the samples were briefly centrifuged and the organic phase (containing the steroids) transferred into another tube and blown to dryness under a stream of nitrogen. The dried extracts were dissolved in 100 μL of mobile phase to be used for automated HPLC analysis. The HPLC system comprised a MR column (4.6 mm $\times$ 50 mm, particle size 2.5 μm; Shimadzu, Tokyo, Japan) as a stationary phase and a mixture of 680/320/1 (v/v/v) Milli-Q water, acetonitrile and trifluoroacetic acid as mobile phase at a flow rate of 1.0 mL/minute. Steroids were detected by UV absorption at 243 nm (Shimadzu, Tokyo, Japan). To quantitate the steroids, peak area ratios versus the internal standard (methylprednisolone) were determined and compared with calibration curves.

Determination of IC$_{50}$ values (potencies) was based on at least five inhibitor concentrations and was derived from the generic equation for enzyme inhibition at fixed substrate concentration $v_i = v_0/(1 + I/\text{IC}_{50})$ with v_i and v_0 being the reaction velocities in the presence or absence of inhibitor respectively, and I being the inhibitor concentration.[41] All analyses were conducted at least in duplicate. IC$_{50}$ values are presented in Table 1.

Molecular Modeling. The CYP11B1 and CYP11B2 protein conformations were extracted from the homology modeling and molecular dynamics study as described in Roumen et al.[29] The protein states sampled during the molecular dynamics were extracted for every 25 ps of the simulation. The inhibitor structures of Table 1 were built with MOE[38] using the MMFF94x force field.

All inhibitors were docked into our CYP11B1 and CYP11B2 models using the program GOLD v3.2[39] using the GoldScore scoring function. The flexible docking of compounds was performed using the parameters from the *default I* settings supplied by GOLD. The GOLD cytochrome P450 parameters were used to obtain ligand poses of the aromatic nitrogen interaction with the protein iron atom.[40] Each ligand was docked in each of the protein states for 50 poses, using the heme iron atom as the definition of the ligand binding site. The docking score of each ligand was averaged over the top 10 different poses using a clustering root-mean-square distance cutoff of 2.0 Å. A binding mode was deemed proper when the aromatic nitrogen atom of the imidazole moiety made an interaction with the heme iron atom at a distance of 2.2 ± 0.2 Å and possessed a $90° \pm 20°$ angle between the Fe−N bond and the heme plane.

Regression Analysis. All regression models were constructed on the basis of a linear correlation using the formula $Y = AX + B$, where A and B are constants, Y is described by compound affinity, and X is described by the docking GoldScore. Compound affinity as used in these equations is expressed as pIC$_{50}$ values. To determine the validity of the regression analysis, leave-one-out (LOO) cross-validation has been performed. Because the data set is of moderate size ($n = 44$), LOO may overestimate the predictivity of the correlation because it only leaves out one compound for internal validation. For this reason, we have chosen to also perform k-fold cross-validation, which uses more compounds for internal validation. If n is the amount of compounds in the data set, the LOO procedure iteratively builds an internal regression model based on $n - 1$ compounds for the prediction of the remaining compound, until each compound has been left out exactly once. The k-fold cross-validation is a variant of the LOO method. For k-fold cross-validation, the data set is randomly partitioned into k sets (folds) of approximately the same size. Then $k - 1$ of these sets are used for the internal prediction of the remaining set, until all k sets have been left out once. Because of the high number of possibilities for the randomized choosing of the k sets, k-fold cross-validation needs to be carried out a sufficient amount of times. Here we have chosen an iterative k-fold analysis of 1000 evaluation runs. In turn, k-fold cross-validation can underestimate the performance of the regression models if too many chemicals are held out for medium size data sets (for instance if 50% is left out). Therefore, we have chosen to partition our data set into folds of nine compounds, which equals just over 20% of the total amount of compounds.

For each of the CYP11B homology models, the following statistical entities have been determined: the squared correlation coefficient, R^2, the Fisher F value, and the cross-validated squared correlation coefficient, q^2, and standard deviation of the predictions, S_{PRESS} for both LOO and k-fold cross-validation, respectively (i.e., LOO: q^2_{LOO}, $S_{\text{PRESS,LOO}}$ and k-fold: $q^2_{k\text{-fold}}$, $S_{\text{PRESS},k\text{-fold}}$). These are indicated in Table 2.

In addition to cross-validation, all data series (x- and y-vectors) have been checked for chance correlation by a process referred to as scrambling, and the regressions of the scrambled y-vectors with the original x-vectors are compared to that of the original y-vector. Because less than 1% of the permutations exceeded correlation with the original vectors and none of the 1000 permutations provided a better correlation than the

original regression model, the likelihood of chance correlations was found to be low (Supporting Information Figures 2 and 3).

Supporting Information Available: Chemical structures of known CYP11B2 inhibitors, results of the Y-scrambling analysis, performance of the GoldScore in various protein conformations, Gold docking values for the different protein models. This material is available free of charge via the Internet at http://pubs.acs.org.

References

(1) Chai, W.; Danser, A. H. Why are mineralocorticoid receptor antagonists cardioprotective? *Naunyn Schmiedeberg's Arch. Pharmacol.* **2006**, *374* (3), 153–162.

(2) Struthers, A. D. Aldosterone: cardiovascular assault. *Am. Heart. J.* **2002**, *144* (5), S2–S7.

(3) Weber, M. A. Clinical implications of aldosterone blockade. *Am. Heart. J.* **2002**, *144* (5), S12–S18.

(4) Lea, W. B.; Kwak, E. S.; Luther, J. M.; Fowler, S. M.; Wang, Z.; Ma, J.; Fogo, A. B.; Brown, N. J. Aldostereone antagonism or synthase inhibition reduces end-organ damage induced by treatment with angiotensin and high salt. *Kidney Int.* **2009**, *75* (9), 936–944.

(5) Sato, A.; Hayashi, K.; Naruse, M.; Saruta, T. Effectiveness of aldosterone blockade in patients with diabetic nephropathy. *Hypertension* **2003**, *41* (1), 64–68.

(6) Schrier, R. W. Water and sodium retention in edematous disorders: role of vasopressin and aldosterone. *Am. J. Med.* **2006**, *119* (7), S47–S53.

(7) Pitt, B.; Williams, G.; Remme, W. J.; Martinez, F.; Lopez-Sendon, J.; Zannad, F.; Neaton, J.; Roniker, B.; Hurley, S.; Burns, D.; Bittman, R.; Kleiman, J. The EPHESUS trial: eplerenone in patients with heart failure due to systolic dysfunction complicating acute myocardial infarction. *Cardiovasc. Drugs Ther.* **2001**, *15* (1), 79–87.

(8) Pitt, B.; Remme, W.; Zannad, F.; Neaton, J.; Martinez, F.; Roniker, B.; Bittman, R.; Hurley, S.; Kleiman, J.; Gatlin, M. Eplerenone, a selective aldosterone blocker, in patients with left ventricular dysfunction after myocardial infarction. *N. Engl. J. Med.* **2003**, *348* (14), 1309–1321.

(9) Hartmann, R. W.; Muller, U.; Ehmer, P. B. Discovery of selective CYP11B2 (aldosterone synthase) inhibitors for the therapy of congestive heart failure and myocardial fibrosis. *Eur. J. Med. Chem.* **2003**, *38* (4), 363–366.

(10) Krum, H.; Nolly, H.; Workman, D; He, W.; Roniker, B.; Krause, S.; Fakouhi, K. Efficacy of eplerenone added to renin-angiotensin blockade in hypertensive patients. *Hypertension* **2002**, *40* (2), 117–123.

(11) Sica, D. A. Pharmacokinetics and pharmacodynamics of mineralocorticoid blocking agents and their effects on potassium homeostasis. *Heart. Failure Rev.* **2005**, *10* (1), 23–29.

(12) Rousseau, M. F.; Gurné, O.; Duprez, D.; van Mieghem, W.; Robert, A.; Ahn, S.; Galanti, L.; Ketelslegers, J.-M. Beneficial neurohormonal profile of spironolactone in severe congestive heart failure. *J. Am. Coll. Cardiol.* **2002**, *40* (9), 1596–1601.

(13) Fisher, A.; Friel, E. C.; Bernhardt, R.; Gomez-Sanchez, C.; Connell, C.; Fraser, J. M. C.; Davies, E. Effects of 18-hydroxylated steroids on corticoid production by human aldosterone synthase and 11beta-hydroxylase. *J. Clin. Encrinol. Metab.* **2001**, *86* (9), 4326–4329.

(14) Okamoto, M.; Nonaka, Y. Molecular biology of rat steroid 11 beta-hydroxylase [P450(11 beta)] and aldosterone synthase [P450(11beta, aldo)]. *Eur. J. Biochem.* **1991**, *202* (3), 897–902.

(15) Fiebeler, A.; Nussberger, J.; Shagdarsuren, E.; Rong, S.; Hilfenhaus, G.; Al-Saadi, N.; Dechend, R.; Wellner, M.; Meiners, S.; Maser-Gluth, C.; Jeng, A. Y.; Webb, R. L.; Luft, F. C.; Muller, D. N. Aldosterone synthase inhibitor ameliorates angiotensin II-induced organ damage. *Circulation* **2005**, *111* (223), 3087–3094.

(16) Minnaard-Huiban, M.; Emmen, J. M. A.; Roumen, L.; Beugels, I. P. E.; Cohuet, G. M. S.; van Essen, H.; Ruijters, E.; Pieterse, K.; Hilbers, P. A. J.; Ottenheijm, H. C. J.; Plate, R.; de Gooyer, M. E.; Smits, J. F. M.; Hermans, J. J. R. Fadrozole Reverses Cardiac Fibrosis in Spontaneously Hypertensive Heart Failure Rats: Discordant

(17) Enantioselectivity Versus Reduction of Plasma Aldosterone. *Endocrinology* **2008**, *149* (1), 28–31.

(17) Huang, B. S.; White, R. A.; Ahmad, M.; Tan, J.; Jeng, A. Y.; Leenen, F. H. Central infusion of aldosterone synthase inhibitor attenuates left ventricular dysfunction and remodeling in rats after myocardial infarction. *Cardiovasc. Res.* **2008**, *81* (3), 574–581.

(18) Menard, J.; Pascoe, L. Can the dextroenantiomer of the aromatase inhibitor fadrozole be useful for clinical investigation of aldosterone-synthase inhibition? *J. Hypertens.* **2006**, *24* (6), 993–997.

(19) Shimoni, Y.; Chen, K.; Emmett, T.; Kargacin, G. Aldosterone and the autocrine modulation of potassium currents and oxidative stress in the diabetic rat heart. *Br. J. Pharmacol.* **2008**, *154* (3), 675–687.

(20) Shiragy, H.; Xue, C. Local renal aldosterone production induces inflammation and matrix formation in kidneys of diabetic rats. *Exp. Physiol.* **2008**, *93* (7), 817–824.

(21) Huang, B. S.; White, R. A.; Jeng, A. Y.; Leenen, F. H. Role of central nervous system aldosterone synthase and mineralocorticoid receptors in salt-induced hypertension in Dahl salt-sensitive rats. *Am. J. Physiol.: Regul. Integr. Comp. Physiol.* **2009**, *296* (4), R994–R1000.

(22) Ulmschneider, S.; Müller-Vieira, U.; Klein, C. D.; Antes, I.; Lengauer, T.; Hartmann, R. W. Synthesis and evaluation of (pyridylmethylene)tetrahydronaphthalenes/-indanes and structurally modified derivatives: potent and selective inhibitors of aldosterone synthase. *J. Med. Chem.* **2005**, *48* (5), 1563–1575.

(23) Voets, M.; Antes, I.; Scherer, C.; Müller-Vieira, U.; Biemel, K.; Barassin, C.; Marchais-Oberwinkler, S.; Hartmann, R. W. Heteroaryl-substituted naphthalenes and structurally modified derivatives: selective inhibitors of CYP11B2 for the treatment of congestive heart failure and myocardial fibrosis. *J. Med. Chem.* **2005**, *48* (21), 6632–6642.

(24) Voets, M.; Antes, I.; Scherer, C.; Müller-Vieira, U.; Biemel, K.; Marchais-Oberwinkler, S.; Hartmann, R. W. Synthesis and evaluation of heteroaryl-substituted dihydronaphthalenes and indenes: potent and selective inhibitors of aldosterone synthase (CYP11B2) for the treatment of congestive heart failure and myocardial fibrosis. *J. Med. Chem.* **2006**, *49* (7), 2222–2231.

(25) Heim, R.; Lucas, S.; Grombein, C. M.; Ries, C.; Schewe, K. E.; Negri, M.; Muller-Vieira, U.; Birk, B.; Hartmann, R. W. Overcoming Undesirable CYP1A2 Inhibition of Pyridylnaphthalene-Type Aldosterone Synthase Inhibitors: Influence of Heteroaryl Derivatization on Potency and Selectivity. *J. Med. Chem.* **2008**, *51* (16), 5064–5074.

(26) de Graaf, C.; Vermeulen, N. P. E.; Feenstra, K. A. Cytochrome P450 in silico: an integrative modeling approach. *J. Med. Chem.* **2005**, *48* (8), 2725–2755.

(27) Lucas, S.; Heim, R.; Negri, M.; Antes, I.; Ries, C.; Schewe, K. E.; Bisi, A.; Gobbi, S.; Hartmann, R. W. Novel aldosterone synthase inhibitors with extended carbocyclic skeleton by a combined ligand-based and structure-based drug design approach. *J. Med. Chem.* **2008**, *51* (19), 6138–6149.

(28) Lucas, S.; Heim, R.; Ries, C.; Schewe, K. E.; Birk, B.; Hartmann, R. W. In vivo active aldosterone synthase inhibitors with improved selectivity: lead optimization providing a series of pyridine substituted 3,4-dihydro-1*H*-quinolin-2-one derivatives. *J. Med. Chem.* **2008**, *51* (24), 8077–8087.

(29) Roumen, L.; Sanders, M. P. A.; Pieterse, K.; Hilbers, P. A. J.; Plate, R.; Custers, E.; de Gooyer, M.; Smits, J. F. M.; Beugels, I.; Emmen, J.; Ottenheijm, H. C. J.; Leysen, D.; Hermans, J. J. R. Construction of 3D models of the CYP11B family as a tool to predict ligand binding characteristics. *J. Comput.-Aided. Mol. Des.* **2007**, *21* (8), 455–471.

(30) Ulmschneider, S.; Müller-Vieira, U.; Mitrenga, M.; Hartmann, R. W.; Oberwinkler-Marchais, S.; Klein, C. D.; Bureik, M.; Bernhardt, R.; Antes, I.; Lengauer, T. Synthesis and evaluation of imidazolylmethylenetetrahydronaphthalenes and imidazolylmethyleneindanes: potent inhibitors of aldosterone synthase. *J. Med. Chem.* **2005**, *48* (6), 1796–1805.

(31) Belkina, N. V.; Lisurek, M.; Ivanov, A. S.; Bernhardt, R. Modelling of three-dimensional structures of cytochromes P450 11B1 and 11B2. *J. Inorg. Biochem.* **2001**, *87* (4), 197–207.

(32) Dorr, H. G.; Kuhnle, U.; Holthausen, H.; Bidlingmaier, F.; Knorr, D. Etomidate: a selective adrenocortical 11 beta-hydroxylase inhibitor. *Klin. Woschenschr.* **1984**, *62* (21), 1011–1013.

(33) Stark, H.; Purand, K.; Hüls, A.; Ligneau, X.; Garbarg, M.; Schwartz, J.-C.; Schunack, W. [^{125}I]Iodoproxyfan and related compounds: a reversible radioligand and novel classes of antagonists with high affinity and selectivity for the histamine H₃ receptor. *J. Med. Chem.* **1996**, *39* (6), 1220–1226.

(34) Erdmann, B.; Denner, K.; Gerst, H.; Lenz, D.; Bernhardt, R. Human adrenal CYP11B1: localisation by in situ hybridization

and functional expression in cell cultures. *Endocr. Res.* **1995**, *21* (1−2), 425–435.

(35) Denner, K.; Doehmer, J.; Bernhardt, R. Cloning of CYP11B1 and CYP11B2 from normal human adrenal and their functional expression in COS-7 and V79 Chinese hamster cells. *Endocr. Res.* **1995**, *21* (1−2), 443–448.

(36) Bottner, B.; Denner, K.; Bernhardt, R. Conferring aldosterone synthesis to human CYP11B1 by replacing key amino acid residues with CYP11B2 ones. *Eur. J. Biochem.* **1998**, *252* (3), 458–466.

(37) Millet, R.; Domarkas, J.; Houssin, R.; Gilleron, P.; Goossens, J.-F.; Chavatte, P.; Logé, C.; Pommery, N.; Pommery, J.; Hénichart, J.-P. Potent and selective farnesyl transferase inhibitors. *J. Med. Chem.* **2004**, *47* (27), 6812–6820.

(38) *MOE* (*The Molecular Operating Environment*) *Version 2007.08*; Chemical Computing Group Inc.: Sherbrooke Street West, Suite 910, Montreal Canada H3A 2R7. http://chemcomp.com

(39) Verdonk, M. L.; Cole, J. C.; Hartshorn, M. J.; Murray, C. W.; Taylor, R. D. Improved protein−ligand docking using GOLD. *Proteins* **2003**, *52* (4), 609–623.

(40) Kirton, B.; Murray, C. W.; Verdonk, M. L.; Taylor, R. D. Prediction of binding modes for ligands in the cytochromes P450 and other heme-containing proteins. *Proteins: Struct., Funct., Bioinf.* **2005**, *58* (4), 836–844.

(41) Cornish-Bowden, A. *Analysis of Enzyme Kinetic Data*; Oxford University Press: Oxford, UK, 1995.